KU LEUVEN

STADIUS
Center for Dynamical Systems, Signal Processing and Data Analytics

Citation/Reference	Verdyck K., Lefevre Y., Tsiaflakis P., Moonen M. (2020), **Per-Tone Precoding and Per-Tone Equalization for OFDM and DMT transmission Systems: Duality, Filter Optimization, and Resource Allocation** IEEE Open Journal of Signal Processing, vol. 1, Nov. 2020, 257-273.
Archived version	Author manuscript: the content is identical to the content of the published paper, but without the final typesetting by the publisher
Published version	https://doi.org/10.1109/OJSP.2020.3035060
Journal homepage	https://signalprocessingsociety.org/publications-resources/ieee-open-journal-signal-processing
Author contact	jeroen.verdyck@esat.kuleuven.be *+ 32 (0)16 32 47 23*
Abstract	OFDM and DMT transmission systems add a cyclic prefix (CP) or zero pad (ZP) to the transmitted signal. Interference-free transmission requires this CP/ZP to be similarly long as the channel impulse response (CIR), reducing the achievable data rate in highly dispersive channels. A first strategy for dealing with long CIRs without increasing the CP/ZP overhead consists of applying a channel shortening filter to the received signal. A second strategy consists of spectral resource allocation, i.e. bit and power allocation to reduce interference. As little effort has been made towards joint channel shortening and resource allocation, a new algorithm to simultaneously optimize the channel shortening per-tone equalization (PTEQ) filters and the resource allocation is presented. In addition, transmitter-side channel shortening filters are considered, more specifically so-called per-tone precoding (PTPC) filters which apply

	the channel shortening filter before the IDFT modulation of the ODFM/DMT transmitter. At first glance, the FIR filter optimization for PTPC seems much more involved than the relatively straightforward FIR filter optimization for PTEQ. However, it will be demonstrated that any OFDM/DMT system with PTPC is — after time-reversing the CIR — equivalent to an OFDM/DMT system employing PTEQ. With this result in hand, systems with PTPC can take full advantage of the straightforward FIR filter optimization in systems with PTEQ, as well as of the aforementioned resource allocation algorithm. Simulation results show that the performance obtained for systems with PTPC is nearly indistinguishable from that obtained for systems with PTEQ, making PTPC an interesting alternative channel shortening strategy.
IR	Klik hier als u tekst wilt invoeren.

(article begins on next page)

Per-Tone Precoding and Per-Tone Equalization for OFDM and DMT Transmission Systems: Duality, Filter Optimization, and Resource Allocation

Jeroen Verdyck, Yannick Lefevre, Paschalis Tsiaflakis, Marc Moonen, *Fellow, IEEE*

OFDM and DMT transmission systems add a cyclic prefix (CP) or zero pad (ZP) to the transmitted signal. Interference-free transmission requires this CP/ZP to be similarly long as the channel impulse response (CIR), reducing the achievable data rate in highly dispersive channels. A first strategy for dealing with long CIRs without increasing the CP/ZP overhead consists of applying a *channel shortening* filter to the received signal. A second strategy consists of spectral *resource allocation*, i.e. bit and power allocation to reduce interference. As little effort has been made towards joint channel shortening and resource allocation, a new algorithm to simultaneously optimize the channel shortening per-tone equalization (PTEQ) filters and the resource allocation is presented.

In addition, transmitter-side channel shortening filters are considered, more specifically so-called per-tone precoding (PTPC) filters which apply the channel shortening filter before the IDFT modulation of the ODFM/DMT transmitter. At first glance, the FIR filter optimization for PTPC seems much more involved than the relatively straightforward FIR filter optimization for PTEQ. However, it will be demonstrated that any OFDM/DMT system with PTPC is — after time-reversing the CIR — equivalent to an OFDM/DMT system employing PTEQ. With this result in hand, systems with PTPC can take full advantage of the straightforward FIR filter optimization in systems with PTEQ, as well as of the aforementioned resource allocation algorithm. Simulation results show that the performance obtained for systems with PTPC is nearly indistinguishable from that obtained for systems with PTEQ, making PTPC an interesting alternative channel shortening strategy.

***Index Terms*—Channel Shortening, DMT, DSL, OFDM, Resource Allocation**

I. Introduction

In OFDM and DMT systems, a cyclic prefix (CP) or zero pad (ZP) is added to the transmitted signal. This CP/ZP serves two purposes: it prevents inter-symbol interference (ISI) between successive symbols, and it suppresses inter-carrier interference (ICI) between subcarriers (a.k.a. tones) of the same symbol. If the CP/ZP is longer than the channel impulse response (CIR), ISI/ICI-free transmission can effectively be achieved. In highly dispersive channels — i.e. channels with a long CIR — ISI/ICI-free transmission will however require a long CP/ZP, reducing the achievable data rate.

In the context of DSL systems specifically, an extension of the G.fast standard [1], [2] has recently been proposed that aims to enable G.fast on lines with a length in excess of 400 m [3]–[7]. Enabling G.fast on such long lines — which can currently only be operated by legacy DSL technologies — will facilitate convergence to a single DSL standard, thereby eliminating co-existence problems between different DSL generations. Key enabling factors for this long-reach (LR) extension of G.fast will be larger constellation sizes [6], a higher maximum aggregate transmit power [3], [6], the application of a looser spectral mask at low frequencies [3], and a longer CP to support longer lines [3]. In the case of G.fast systems however, where the same CP length is applied across all users in both upstream and downstream [2], using a longer CP to support longer lines will inevitably reduce the data rate on shorter lines. Based on this observation, interest in techniques dealing with long CIRs without increasing the CP overhead has recently resurfaced.[1]

A first strategy to mitigate the effects of ISI/ICI in highly dispersive channels without employing an excessively long CP/ZP consists of channel shortening. Chow *et al.* [8] have proposed the use of a finite impulse response (FIR) time-domain equalization (TEQ) filter to shorten the CIR. Van Acker *et al.* [9] have proposed moving this TEQ filter into the frequency domain — i.e. to after the DFT demodulation of the OFDM/DMT receiver — and allowing a different FIR filter for each subcarrier, which can be implemented without increasing the run-time complexity as compared to TEQ. The resulting channel shortening strategy is referred to as per-tone equalization (PTEQ). While PTEQ indeed requires more memory than TEQ due to the increased number of FIR filter coefficients, the main advantages are that 1) maximizing the SNR on each subcarrier individually leads to a straightforward FIR filter optimization, and 2) PTEQ is a generalization of TEQ, i.e. any specific TEQ filter can be equivalently implemented as a PTEQ filter whereas the reverse is not true. As such, PTEQ provides an upper bound on the performance of TEQ.

A second method to mitigate the effects of ISI/ICI without employing an excessively long prefix consists of spectral resource allocation, i.e. bit and power allocation [10], which

J. Verdyck and M. Moonen are with the STADIUS Center for Dynamical Systems, Signal Processing and Data Analytics in the Department of Electrical Engineering (ESAT), KU Leuven, 3000 Leuven, Belgium.

Y. Lefevre and P. Tsiaflakis are with the Fixed Networks Research Antwerp Team of Nokia Bell Labs, 2018 Antwerp, Belgium.

This research work was carried out at the ESAT Laboratory of KU Leuven, in the frame of Fonds de la Recherche Scientifique (FNRS) and Fonds Wetenschappelijk Onderzoek Vlaanderen (FWO) EOS Project nr. 30452698 "(MUSE-WINET) MUlti-SErvice WIreless NETwork", FWO Research Project nr. G.0B1818N "Real-time adaptive cross-layer dynamic spectrum management for fifth generation broadband copper access networks", Vlaams Agentschap Innoveren & Ondernemen (VLAIO) O&O Project nr. HBC.2017.1007 "(MIA) Multi-gigabit Innovations in Access". The scientific responsibility is assumed by its authors.

[1] Even though the current interest in this subject is mainly coming from the DSL community, the theoretical and algorithmic developments in this paper will be kept general such that these can be applied to other OFDM or DMT-based systems as well.

exploits the fact that not all subcarriers are equally susceptible to ISI/ICI [11]. Algorithms for resource allocation have been considered in [10], [12] for ISI/ICI due to an insufficiently long prefix, and in [13]–[15] for ISI/ICI due to asynchronous transmissions.

While both aforementioned ISI/ICI mitigation methods have received significant attention in literature, it is remarkable that little effort has been made towards a joint channel shortening and resource allocation. To the best of the authors' knowledge, only [16] has addressed the issue by considering sparse PTEQ filter coefficient optimization combined with a power allocation method. However, the proposed method in [16] ignores the ICI while executing an exhaustive search over a discrete set of power levels to obtain a power allocation, which can lead to poor performance in the presence of ISI/ICI [13]. It is deemed that *optimal* power allocation algorithms would be more appropriate to guide the design of power allocation heuristics towards enhanced performance. In this paper, a new algorithm to simultaneously optimize the PTEQ filter and the resource allocation is therefore presented.

In addition, transmitter-side channel shortening is considered. Time-domain precoding (TPC) filters were first considered in [17]. Similar to PTEQ, one can move the TPC filter into the frequency domain — i.e. to before the IDFT modulation of the OFDM/DMT transmitter — without a significant impact on run-time complexity, yielding a channel shortening algorithm that will be referred to as per-tone precoding (PTPC).[2]

At first glance, the FIR filter optimization for PTPC seems much more involved than the relatively straightforward FIR filter optimization for PTEQ. In addition, the more involved PTPC filter optimization complicates the resource allocation problem. However, it is demonstrated in this paper that any OFDM/DMT system with (P)TPC is — after time-reversing the CIR — equivalent to an OFDM/DMT system employing (P)TEQ. The obtained equivalence result is rooted in MAC-BC duality theory [19]–[21], and will be referred to as PTEQ-PTPC duality. With this duality result in hand, PTPC systems can take full advantage of the straightforward FIR filter optimization in PTEQ systems, as well as of the developed resource allocation algorithm.

Contributions

A joint PTEQ filter optimization and resource allocation algorithm is proposed for OFDM/DMT systems with PTEQ, which provably converges to a stationary point of the considered rate maximization problem and obtains a sufficient accuracy after only a few iterations. Moreover, the use of an iterative water filling (IWF) algorithm is proposed as a resource allocation heuristic for PTEQ systems. Simulation results show that IWF achieves good performance when the ISI/ICI is sufficiently suppressed by the PTEQ filter.

In addition, the use of a transmitter-side channel shortening per-tone precoder (PTPC) is proposed. A duality result is proven between the proposed PTPC filter and the well-studied PTEQ filter. A joint PTPC filter optimization and resource allocation algorithm is developed by using this duality result. Simulation results show that the performance obtained for OFDM/DMT systems with PTPC is nearly indistinguishable from that obtained for OFDM/DMT systems with PTEQ.

Notation

Throughout the paper, matrices will be bold-faced and non-italicized. Vectors will be bold-faced and italicized. Zero-based indexing will be used when addressing vector and matrix elements, i.e. for any $N \times M$ matrix $\mathbf{A}$ we have the following

$$\begin{aligned} \mathbf{A}^{\mathrm{T}} &= [(\mathrm{row}_0(\mathbf{A}))^{\mathrm{T}}, \ldots, (\mathrm{row}_{N-1}(\mathbf{A}))^{\mathrm{T}}]\,; \\ \mathbf{A} &= [\mathrm{col}_0(\mathbf{A}), \ldots, \mathrm{col}_{M-1}(\mathbf{A})]\,; \\ [\mathbf{A}]_{n,m} &= \mathrm{row}_n\left(\mathrm{col}_m(\mathbf{A})\right). \end{aligned}$$

The Hadamard product of matrices $\mathbf{A}$ and $\mathbf{B}$ will be denoted as $\mathbf{A} \circ \mathbf{B}$. A diagonal matrix with its diagonal given by $\boldsymbol{a}$ will be denoted as $\mathrm{diag}\{\boldsymbol{a}\}$. The matrices $\mathbf{I}_N$ and $\mathbf{0}_{N\times M}$ will respectively denote the $N\times N$ identity matrix and the $N\times M$ all-zeros matrix. The dimension subscripts in $\mathbf{I}_N$ and $\mathbf{0}_{N\times M}$ will be omitted when they can be derived from the context. Moreover, $\mathbf{A}^{\mathrm{T}}$, $\mathbf{A}^{*}$, and $\mathbf{A}^{\mathcal{H}}$ will respectively denote the transpose, the complex conjugate, and the Hermitian transpose of $\mathbf{A}$. The matrix inequality $\mathbf{A} \succeq \mathbf{B}$ will denote that $(\mathbf{A} - \mathbf{B})$ is positive semidefinite, and the vector inequality $\boldsymbol{a} \geq \boldsymbol{b}$ will denote that $\boldsymbol{a}$ is element-wise larger than $\boldsymbol{b}$. The Frobenius norm of a matrix will be denoted as $|a|$. The expected value operator will be denoted as $\mathbb{E}[\,]$. Finally, the sets of real, positive real, and strictly positive real numbers will respectively be denoted as $\mathbb{R}$, $\mathbb{R}_{+}$, and $\mathbb{R}_{++}$.

II. System Model

Fig. 1 depicts a general OFDM system model consisting of an encoder $\mathbf{T}$, a decoder $\mathbf{R}$, a serial-to-parallel (S/P) and parallel-to-serial (P/S) converter, and a frequency-selective channel that is modeled as an FIR filter $H(z) = \sum_{k'=0}^{L} z^{-k'}\, h[k']$. It is noted that a different sample index k' is used between the P/S converter and the S/P converter, as they respectively execute an upsampling and a downsampling operation. The noise samples $z[k']$ are assumed to be i.i.d. and Gaussian,[3] with an average power given by $\mathbb{E}\left[|z[k']|^2\right] = \sigma^2$. The complex vectors $\boldsymbol{X}[k] \triangleq [X_0[k], \ldots, X_{N-1}[k]]^{\mathrm{T}}$ and $\hat{\boldsymbol{X}}[k] \triangleq [\hat{X}_0[k], \ldots, \hat{X}_{N-1}[k]]^{\mathrm{T}}$ respectively denote the frequency-domain input and output symbol, where N is the employed DFT size (cf. infra). The covariance matrix of $\boldsymbol{X}[k]$ is

$$\mathbb{E}\left[\boldsymbol{X}[k]\,\boldsymbol{X}[l]^{\mathcal{H}}\right] = \begin{cases} \mathrm{diag}\{\boldsymbol{S}\} & \text{when } k = l \\ \mathbf{0}_N & \text{when } k \neq l \end{cases} \tag{1}$$

with $\boldsymbol{S} \triangleq [S_0, \ldots, S_{N-1}]^{\mathrm{T}} \in \mathbb{R}_{+}^{N}$ the power allocation vector.

In Section II-A and Section II-B, two OFDM flavors are reviewed, namely Cyclic Prefix (CP) OFDM and Zero-Padded (ZP) OFDM. In Section II-C and Section II-D, PTEQ and PTPC are introduced.

[2]The considered PTPC has actually first been introduced in the context of per-tone spectral shaping [18], but its use for channel shortening has not been considered before.

[3]While certainly possible, extending the models and algorithms in this paper to include colored noise would further obfuscate the derivations, and is therefore considered to be out-of-scope.

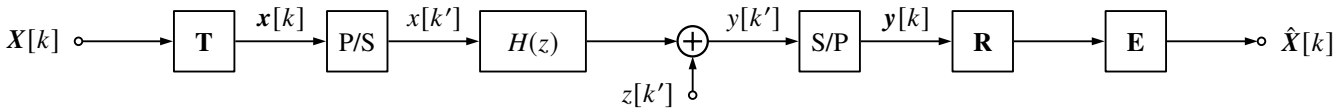

Fig. 1. A general OFDM/DMT transceiver model.

Discrete MultiTone

When appropriate, it is indicated how to adapt the presented OFDM system model, algorithms and results to DMT systems. DMT systems operate at baseband, resulting in the requirement that the transmitted signal $x[k']$ be real. As will be evident from the definitions of $\mathbf{T}$ in Sections II-A, II-B and II-D, this requirement is satisfied if and only if $\boldsymbol{X}[k]$ admits the following Hermitian symmetric structure:

$$X_{n^*}[k] = (X_n[k])^*, \forall n,$$

where — with a slight abuse of notation — n^* is the index of the subcarrier that is the Hermitian symmetric of n, i.e. where $n^* \triangleq (N-n) \mod N$. Note that only even DFT sizes N will be considered in the context of DMT systems. Assuming that the real and imaginary part of $X_n[k]$ are i.i.d. $\forall n \in \{1,\ldots,N/2-1\}$, it is readily seen that $\mathbb{E}\,[X_{n^*}[k]\,(X_n[k])^*] = 0$ $\forall n \in \{0,\ldots,N/2\}$. The covariance matrix of $\boldsymbol{X}[k]$ therefore still follows (1). The power vector $\boldsymbol{S}$ will however admit the same Hermitian symmetric structure as $\boldsymbol{X}[k]$, i.e. $S_n = S_{n^*}$.

A. Cyclic Prefix OFDM (CP-OFDM)

The CP-OFDM transmitter transforms the input symbols $\boldsymbol{X}[k]$ to the time domain by application of the IDFT, and adds a cyclic prefix (CP) to the result. The k-th transmitted time-domain symbol is thus

$$\boldsymbol{x}[k] = \mathbf{T}^{\text{CP}}\,\boldsymbol{X}[k] = \left[\begin{array}{c|c} \mathbf{0} & \mathbf{I}_\nu \\ \hline & \mathbf{I}_N \end{array}\right] \mathcal{I}_N\,\boldsymbol{X}[k], \tag{2}$$

with ν the cyclic prefix length, and $\mathcal{I}_N$ the N-point IDFT matrix. The following definitions are used for $\mathcal{I}_N$ and the corresponding N-point DFT matrix $\mathcal{F}_N$.

$$\mathcal{I}_N \triangleq \mathcal{F}_N^{-1} \qquad [\mathcal{F}_N]_{n,m} \triangleq \alpha^{-n\,m} \qquad \alpha \triangleq e^{2\pi j/N} \tag{3}$$

The time-domain symbol length is denoted as $s = N+\nu$. At the receiver, the cyclic prefix is removed from the k-th received signal $\boldsymbol{y}[k] = \left[y_0[k],\ldots,y_{s-1}[k]\right]^{\text{T}}$ before application of the DFT and frequency-domain equalization (FEQ). As such, the output symbol $\hat{\boldsymbol{X}}[k]$ can be expressed as

$$\hat{\boldsymbol{X}}[k] = \mathbf{E}\,\mathbf{R}^{\text{CP}}\,\boldsymbol{y}[k] = \mathbf{E}\,\mathcal{F}_N \left[\begin{array}{cc} \mathbf{0}_{N\times\nu} & \mathbf{I}_N \end{array}\right] \boldsymbol{y}[k], \tag{4}$$

with $\mathbf{E}$ the diagonal FEQ matrix. Assuming perfect synchronization between the transmitter-side P/S converter and receiver-side S/P converter, each $\hat{X}_n[k]$ will be free of ISI/ICI if $\nu \geq L$.

B. Zero-Padded OFDM (ZP-OFDM)

The ZP-OFDM transmitter adds a zero pad instead of a cyclic prefix. The k-th time-domain symbol is thus

$$\boldsymbol{x}[k] = \mathbf{T}^{\text{ZP}}\,\boldsymbol{X}[k] = \left[\begin{array}{c} \mathbf{I}_N \\ \hline \mathbf{0}_{\nu\times N} \end{array}\right] \mathcal{I}_N\,\boldsymbol{X}[k], \tag{5}$$

with ν the pad length. A ZP-OFDM-OLA receiver is assumed here, which adds the first ν samples of the received signal $\boldsymbol{y}[k]$ to the last samples of $\boldsymbol{y}[k]$ before application of the DFT and FEQ [22]:

$$\hat{\boldsymbol{X}}[k] = \mathbf{E}\,\mathbf{R}^{\text{ZP}}\,\boldsymbol{y}[k] = \mathbf{E}\,\mathcal{F}_N \left[\begin{array}{c|c} \mathbf{0} & \\ \mathbf{I}_\nu & \mathbf{I}_N \end{array}\right] \boldsymbol{y}[k]. \tag{6}$$

Assuming perfect synchronization between the P/S and S/P blocks, each $\hat{X}_n[k]$ will again be free of ISI/ICI if $\nu \geq L$.[4]

C. Per-Tone Equalization

PTEQ [9] is described here by first introducing TEQ in the receiver, and then deriving the PTEQ from this TEQ. The idea of TEQ is to apply a filter $W(z) = \sum_{k'=0}^{T} z^{-k'}\,w[k']$ to $y[k']$ in order to shorten the CIR, thereby reducing the required ν for ISI/ICI-free transmission and hence the corresponding data rate overhead. The receiver with TEQ thus executes the following operation:

$$\hat{\boldsymbol{X}}[k] = \mathbf{E}\,\mathbf{R} \begin{bmatrix} \boxed{\boldsymbol{w}^{\text{T}}} & 0 & \cdots \\ 0 & \ddots & \ddots \\ \vdots & \ddots & \boxed{\boldsymbol{w}^{\text{T}}} \end{bmatrix} \tilde{\boldsymbol{y}}[k], \tag{7}$$

where $\tilde{\boldsymbol{y}}[k] \triangleq \left[y_{s-T}[k-1],\ldots,y_{s-1}[k-1],(\boldsymbol{y}[k])^{\text{T}}\right]^{\text{T}}$ is the extended received signal, where $\boldsymbol{w}^{\text{T}} \triangleq \left[w[T],\ldots,w[0]\right]$ contains the TEQ filter coefficients, and where $\mathbf{R}$ can be either $\mathbf{R}^{\text{CP}}$ or $\mathbf{R}^{\text{ZP}}$. From here on, it will not be specified explicitly whether $\mathbf{R}$, $\mathbf{T}$, or their derived variables correspond to a CP-OFDM or to a ZP-OFDM system in equations that are valid for both.

PTEQ is based on transferring the TEQ to the frequency domain — i.e. to after the DFT operation [9] — which can be done based on the following reformulation of equation (7), where $E_n \triangleq \left[\mathbf{E}\right]_{n,n}$.

$$\hat{X}_n[k] = E_n\,\boldsymbol{w}^{\text{T}} \underbrace{\begin{bmatrix} \boxed{\text{row}_n(\mathbf{R})} & 0 & \cdots \\ 0 & \ddots & \ddots \\ \vdots & \ddots & \boxed{\text{row}_n(\mathbf{R})} \end{bmatrix}}_{\triangleq \mathbf{R}_n} \tilde{\boldsymbol{y}}[k] \tag{8}$$

[4]The ZP-OFDM-OLA receiver from [22] adds the last ν samples of $\boldsymbol{y}[k]$ to the first samples of $\boldsymbol{y}[k]$, as opposed to what is done in (6). The two are however equivalent up to a phase shift of the elements of $\mathbf{E}$ due to the DFT shift theorem [23, Eq. 3.2-4].

The receiver with PTEQ is then obtained by effectively allowing each subcarrier to have its own TEQ — implemented as a T-th order FEQ filter with filter coefficients $\boldsymbol{w}_n^{\mathcal{H}} \triangleq \left[w_n[T], \ldots, w_n[0]\right]$ — by removing the constraint that $\forall n : \boldsymbol{w}_n^{\mathcal{H}} = E_n \boldsymbol{w}^{\mathsf{T}}$ for one overall TEQ filter $\boldsymbol{w}$. The output symbol on the n-th subcarrier of a receiver with PTEQ is thus given as

$$\hat{X}_n[k] = \boldsymbol{w}_n^{\mathcal{H}} \mathbf{R}_n \, \tilde{\boldsymbol{y}}[k]. \tag{9}$$

From (9), it may appear that PTEQ brings a significant complexity increase w.r.t. TEQ as it seems to require $T+1$ DFT operations (whereas TEQ demands only a single DFT). Fortunately, when $\mathbf{R}_n$ corresponds to the CP-OFDM decoder of Section II-A or the ZP-OFDM decoder of Section II-B, one can reduce the $T+1$ DFT operations back to one by decomposing $\mathbf{R}_n$ into a lower triangular matrix and a sparse matrix as in [9], [18], i.e.

$$\mathbf{R}_n^{\text{ZP}} = \underbrace{\begin{bmatrix} \alpha^{0n} & \cdots & 0 \\ \vdots & \ddots & \vdots \\ \alpha^{Tn} & \cdots & \alpha^{0n} \end{bmatrix}}_{\triangleq \mathbf{L}_n} \underbrace{\left[\begin{array}{c|c|c} \boxed{\text{row}_n(\mathbf{R}^{\text{ZP}})} & & \mathbf{0} \\ -\alpha^{(\nu+1)n}\mathbf{I}_T & \mathbf{0} & \alpha^n \mathbf{I}_T \end{array}\right]}_{\triangleq \underline{\mathbf{R}}_n^{\text{ZP}}} \tag{10a}$$

for ZP-OFDM and

$$\mathbf{R}_n^{\text{CP}} = \begin{bmatrix} \alpha^{0n} & \cdots & 0 \\ \vdots & \ddots & \vdots \\ \alpha^{Tn} & \cdots & \alpha^{0n} \end{bmatrix} \underbrace{\left[\begin{array}{c|c|c} \boxed{\text{row}_n(\mathbf{R}^{\text{CP}})} & & \mathbf{0} \\ \mathbf{0}_{T\times\nu} & -\alpha^n \mathbf{I}_T \quad \mathbf{0} & \alpha^n \mathbf{I}_T \end{array}\right]}_{\triangleq \underline{\mathbf{R}}_n^{\text{CP}}} \tag{10b}$$

for CP-OFDM where $\underline{\mathbf{R}}_n$ corresponds to a single DFT together with the usage of T so-called difference terms. With this decomposition, equation (9) becomes

$$\hat{X}_n[k] = \boldsymbol{v}_n^{\mathcal{H}} \underline{\mathbf{R}}_n \, \tilde{\boldsymbol{y}}[k], \tag{11}$$

where $\boldsymbol{v}_n \triangleq \mathbf{L}_n^{\mathcal{H}} \boldsymbol{w}_n$. An in-depth run-time complexity analysis of PTEQ is provided in [9].

Finally, an expression for the signal-to-interference-plus-noise ratio (SINR) on each subcarrier is established. The starting point for this expression is the complete input-output equation as in (12) at the top of the next page,[5] where $\boldsymbol{h} \triangleq \left[h[L], \ldots, h[0]\right]$. With $\boldsymbol{X}[k]$ the symbol of interest and $\boldsymbol{X}[k-1]$,$\boldsymbol{X}[k+1]$ its neighboring symbols, this equation accurately models the ICI, as well as all the ISI originating from the neighboring symbols. When L is very large, more neighboring symbols can be included in the equation [24]. Letting δ denote the so-called synchronization delay, the dimensions of $\mathbf{O}_1$ and $\mathbf{O}_2$ become $(s+T)\times(s-L-T+\delta)$ and $(s+T)\times(s-\delta)$, respectively. When $\delta = 0$, this choice for the dimensions of $\mathbf{O}_1$ and $\mathbf{O}_2$ ensures that $y_0[k]$ is the first sample that has a contribution from $\boldsymbol{X}[k]$. By separating the Toeplitz matrix $\mathbf{H}_\delta$, which has dimensions $(s+T)\times(3s)$, into three $(s+T)\times s$ matrices $\{\mathbf{H}_\delta[l]\}_{l=\{-1,0,1\}}$, equation (12) can be rewritten as

$$\hat{X}_n[k] = \boldsymbol{v}_n^{\mathcal{H}} \underline{\mathbf{R}}_n \sum_{l=-1}^{1} \mathbf{H}_\delta[l] \, \mathbf{T} \, \boldsymbol{X}[k+l] + \boldsymbol{v}_n^{\mathcal{H}} \underline{\mathbf{R}}_n \, \tilde{\boldsymbol{z}}[k]. \tag{13}$$

Moreover, by defining the $(T+1)\times 1$ residual channel vectors $\boldsymbol{h}_{nm}[l]$ and residual channel matrices $\mathbb{H}_{nm}$ as

$$\boldsymbol{h}_{nm}[l] \triangleq \underline{\mathbf{R}}_n \, \mathbf{H}_\delta[l] \, \text{col}_m(\mathbf{T}), \tag{14a}$$

$$\mathbb{H}_{nm} \triangleq \begin{cases} \left[\begin{array}{c|c|c} \boldsymbol{h}_{nm}[-1] & \boldsymbol{h}_{nm}[0] & \boldsymbol{h}_{nm}[1] \end{array}\right] & \text{when } n \neq m \\ \left[\begin{array}{c|c} \boldsymbol{h}_{nn}[-1] & \boldsymbol{h}_{nn}[1] \end{array}\right] & \text{when } n = m \end{cases}, \tag{14b}$$

and introducing $\boldsymbol{h}_n \triangleq \boldsymbol{h}_{nn}[0]$ — with $\mathbb{E}\left[|z[k']|^2\right] = \sigma^2$ and $\mathbb{E}\left[\boldsymbol{X}[k]\,\boldsymbol{X}[l]^{\mathcal{H}}\right]$ conforming to (1) — the following SINR expression is straightforwardly obtained for subcarrier n:

$$\gamma_n(\boldsymbol{S}, \boldsymbol{v}_n) = \frac{S_n \left|\boldsymbol{v}_n^{\mathcal{H}} \boldsymbol{h}_n\right|^2}{\sum_{m=0}^{N-1} S_m \left|\boldsymbol{v}_n^{\mathcal{H}} \mathbb{H}_{nm}\right|^2 + \sigma^2 \left|\boldsymbol{v}_n^{\mathcal{H}} \underline{\mathbf{R}}_n\right|^2}. \tag{15}$$

D. Per-Tone Precoding

PTPC is described here by first introducing TPC in the transmitter, and then deriving the PTPC from this TPC. The signal flow graph of a transmitter (represented as a synthesis filter bank) with TPC is given in Fig. 2. The filters $F_n(z)$ in Fig. 2 realize (2) or (5), and are described by

$$F_n(z) = \left[1, z^{-1}, \ldots, z^{-(s-1)}\right] \text{col}_n(\mathbf{T}). \tag{16}$$

The TPC filter $W(z) = \sum_{k'=0}^{T} z^{-k'} \, w[k']$ in Fig. 2 is, analogous to the TEQ in Section II-C, aimed at shortening the CIR. The TPC transmitter applies the following filter to each expanded (upsampled) input symbol stream $[X_n[k]]_{\uparrow s}$:

$$P_n(z) = \left[1, z^{-1}, \ldots, z^{-(s+T-1)}\right] \underbrace{\begin{bmatrix} \boxed{\text{col}_n(\mathbf{T})} & 0 & \cdots \\ & & \ddots \\ & \ddots & \boxed{\text{col}_n(\mathbf{T})} \\ 0 & & \\ \vdots & \ddots & \end{bmatrix}}_{\triangleq \mathbf{T}_n} \bar{\boldsymbol{w}}, \tag{17}$$

with $\bar{\boldsymbol{w}} \triangleq \left[w[0], \ldots, w[T]\right]^{\mathsf{T}}$. The overbar in $\bar{\boldsymbol{w}}$ indicates that PTPC filter coefficients are considered. The same overbar-notation will be used to indicate PTPC channel matrices, SINRs and, symbol powers. The transmitter with PTPC is then obtained by allowing a different, possibly complex $\bar{\boldsymbol{w}}_n$ on each subcarrier n. The transmitter with PTPC thus applies the following filter to each expanded input symbol stream $[X_n[k]]_{\uparrow s}$.

$$P_n(z) = \left[1, z^{-1}, \ldots, z^{-(s+T-1)}\right] \mathbf{T}_n \, \bar{\boldsymbol{w}}_n \tag{18}$$

A low-complexity implementation of the resulting filter structure is proposed in [18], albeit in the context of per-

[5] In this equation, the PTEQ receiver as in (11) has been employed because it enables an efficient implementation of the SINR calculation, as well as of the resource allocation algorithm from Section III. This choice has no bearing on the derivations in Sections III and IV, i.e. employing the PTEQ as in (9) would yield equivalent theories, algorithms, and results.

$$\hat{X}_n[k] = \boldsymbol{v}_n^{\mathcal{H}} \underline{\mathbf{R}}_n \underbrace{\left[\begin{array}{c|ccc|c} \mathbf{O}_1 & \boxed{\boldsymbol{h}} & 0 & \cdots & \\ & 0 & \ddots & \ddots & \mathbf{O}_2 \\ & \vdots & \ddots & \boxed{\boldsymbol{h}} & \end{array}\right]}_{\triangleq \mathbf{H}_\delta} \left[\begin{array}{ccc} \mathbf{T} & & \\ & \mathbf{T} & \\ & & \mathbf{T} \end{array}\right] \left[\begin{array}{c} \boldsymbol{X}[k-1] \\ \boldsymbol{X}[k] \\ \boldsymbol{X}[k+1] \end{array}\right] + \boldsymbol{v}_n^{\mathcal{H}} \underline{\mathbf{R}}_n \, \tilde{\boldsymbol{z}}[k] \tag{12}$$

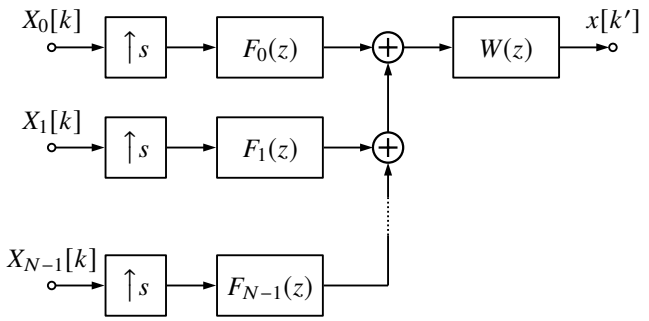

Fig. 2. Synthesis filter bank representation of the CP-OFDM (including P/S converter), concatenated with a Time-domain PreCoding (TPC) filter $W(z)$.

subcarrier spectral shaping.[6] This low complexity implementation is based on the decomposition of $\mathbf{T}_n$ into a sparse matrix and an upper triangular matrix [9], [18]:

$$\mathbf{T}_n^{\text{ZP}} = \underbrace{\left[\begin{array}{cc} \boxed{\text{col}_n(\mathbf{T}^{\text{ZP}})} & \begin{array}{c} -N^{-1}\alpha^{-n}\,\mathbf{I}_T \\ \mathbf{0}_{(N-T)\times T} \\ N^{-1}\alpha^{-n}\,\mathbf{I}_T \\ \mathbf{0}_{(\nu-T)\times T} \end{array} \\ \hline \mathbf{0}_{T\times 1} & \mathbf{0}_T \end{array}\right]}_{\triangleq \underline{\mathbf{T}}_n^{\text{ZP}}} \underbrace{\left[\begin{array}{ccc} \alpha^{-0n} & \cdots & \alpha^{-Tn} \\ \vdots & \ddots & \vdots \\ 0 & \cdots & \alpha^{-0n} \end{array}\right]}_{\triangleq \mathbf{U}_n} \tag{19a}$$

for ZP-OFDM and

$$\mathbf{T}_n^{\text{CP}} = \underbrace{\left[\begin{array}{cc} \boxed{\text{col}_n(\mathbf{T}^{\text{CP}})} & -N^{-1}\alpha^{-(\nu+1)n}\,\mathbf{I}_T \\ \hline \mathbf{0} & N^{-1}\alpha^{-n}\,\mathbf{I}_T \end{array}\right]}_{\triangleq \underline{\mathbf{T}}_n^{\text{CP}}} \left[\begin{array}{ccc} \alpha^{-0n} & \cdots & \alpha^{-Tn} \\ \vdots & \ddots & \vdots \\ 0 & \cdots & \alpha^{-0n} \end{array}\right] \tag{19b}$$

for CP-OFDM. Using this decomposition, (18) can be rewritten as

$$P_n(z) = \left[1, z^{-1}, \ldots, z^{-(s+T-1)}\right] \underline{\mathbf{T}}_n \, \bar{\boldsymbol{v}}_n. \tag{20}$$

where $\bar{\boldsymbol{v}}_n \triangleq \mathbf{U}_n \, \bar{\boldsymbol{w}}_n$ now contains the PTPC filter coefficients.

Finally, an expression for the SINR on each subcarrier is established. The starting point for this expression is the input-output equation as in (21) at the top of the next page, where $\mathbf{P}$ is defined as

$$\text{col}_n(\mathbf{P}) \triangleq \underline{\mathbf{T}}_n \, \bar{\boldsymbol{v}}_n. \tag{22}$$

The dimensions of $\mathbf{O}_3$ and $\mathbf{O}_4$ are chosen as $s \times (s+T-L+\delta)$ and $s \times (s-\delta)$, respectively. With $\delta = 0$, this choice ensures that $y_0[k]$ is the $(T+1)$-th sample that has a contribution from $\boldsymbol{X}[k]$. By separating the Toeplitz matrix $\bar{\mathbf{H}}_\delta$, which has dimensions $s \times (3s+T)$, into three overlapping $s \times (s+T)$ matrices $\{\bar{\mathbf{H}}_\delta[l]\}_{l=\{-1,0,1\}}$,[7] the channel model in (21) can equivalently be written as

$$\hat{\boldsymbol{X}}[k] = \mathbf{E}\,\mathbf{R} \sum_{l=-1}^{1} \bar{\mathbf{H}}_\delta[l]\,\mathbf{P}\,\boldsymbol{X}[k+l] + \mathbf{E}\,\mathbf{R}\,\boldsymbol{z}[k]. \tag{23}$$

By defining the $(T+1)\times 1$ residual channel vectors $\bar{\boldsymbol{h}}_{nm}[l]$ and residual channel matrices $\bar{\mathbb{H}}_{nm}$ as

$$\bar{\boldsymbol{h}}_{nm}[l] \triangleq \underline{\mathbf{T}}_m^{\mathcal{H}} \left(\bar{\mathbf{H}}_\delta[l]\right)^{\mathcal{H}} \left(\text{row}_n(\mathbf{R})\right)^{\mathcal{H}}, \tag{24a}$$

$$\bar{\mathbb{H}}_{nm} \triangleq \begin{cases} \left[\begin{array}{c|c|c} \bar{\boldsymbol{h}}_{nm}[-1] & \bar{\boldsymbol{h}}_{nm}[0] & \bar{\boldsymbol{h}}_{nm}[1] \end{array}\right] & \text{when } i \neq j \\ \left[\begin{array}{c|c} \bar{\boldsymbol{h}}_{nn}[-1] & \bar{\boldsymbol{h}}_{nn}[1] \end{array}\right] & \text{when } i = j \end{cases}, \tag{24b}$$

and introducing $\bar{\boldsymbol{h}}_n \triangleq \bar{\boldsymbol{h}}_{nn}[0]$ — with $\mathbb{E}\left[|z[k']|^2\right] = \sigma^2$ and $\mathbb{E}\left[\boldsymbol{X}[k]\,\boldsymbol{X}[l]^{\mathcal{H}}\right]$ conforming to (1) — the following SINR expression is straightforwardly obtained for subcarrier n:

$$\bar{\gamma}_n(\bar{\boldsymbol{S}}, \bar{\boldsymbol{v}}_0, \ldots, \bar{\boldsymbol{v}}_{N-1}) = \frac{\bar{S}_n \left|\bar{\boldsymbol{v}}_n^{\mathcal{H}} \bar{\boldsymbol{h}}_n\right|^2}{\sum_{m=0}^{N-1} \bar{S}_m \left|\bar{\boldsymbol{v}}_m^{\mathcal{H}} \bar{\mathbb{H}}_{nm}\right|^2 + \sigma^2 \,|\,\text{row}_n(\mathbf{R})|^2}, \tag{25}$$

where for PTPC, the power allocation vector and its elements are denoted as $\bar{\boldsymbol{S}} \triangleq [\bar{S}_0, \ldots, \bar{S}_{N-1}]^{\text{T}}$.

Discrete MultiTone

DMT systems with PTPC should enforce $\bar{\boldsymbol{w}}_{n^*} = \bar{\boldsymbol{w}}_n^*$ or $\bar{\boldsymbol{v}}_{n^*} = \bar{\boldsymbol{v}}_n^*$ to guarantee that $x[k'] \in \mathbb{R}$.

E. Performance metrics

The achievable bit loading b, which is assumed here to be a continuous variable, will be modeled as a function of the SINR γ as

$$b(\gamma) = \log_2\left(1 + \Gamma^{-1}\gamma\right), \tag{26}$$

where $\log_2()$ is the binary logarithm and Γ is the so-called SNR-gap to capacity — the inclusion of which results in a more accurate model of the relation between the constellation size and the SINR required to achieve a target bit error rate (BER) for practical modulation and coding schemes [27]–[29].

[6] Spectral shaping is usually implemented as a time-domain windowing operation. The windowing operation in OFDM-based systems, e.g. as described in [2], [25], is equivalent to applying frequency-shifted versions of a single short prototype filter $W_0(z)$ to the output of each filter $F_n(z)$ in Fig. 2 [26]. In this context, the authors of [18] proposed to use per-subcarrier spectral shaping filters to improve on the performance of time-domain windowing.

[7] Each pair of matrices $\{\bar{\mathbf{H}}_\delta[-1], \bar{\mathbf{H}}_\delta[0]\}$ and $\{\bar{\mathbf{H}}_\delta[0], \bar{\mathbf{H}}_\delta[1]\}$ has T columns in common.

$$\hat{\boldsymbol{X}}[k] = \mathbf{E}\,\mathbf{R}\underbrace{\left[\begin{array}{c|ccc|c} \mathbf{O}_3 & \boxed{\boldsymbol{h}} & 0 & \cdots & \mathbf{O}_4 \\ & 0 & \ddots & \ddots & \\ & \vdots & \ddots & \boxed{\boldsymbol{h}} & \end{array}\right]}_{\triangleq \bar{\mathbf{H}}_\delta}\left[\begin{array}{ccc} \boxed{\mathbf{P}} & \mathbf{0}_{s\times N} & \mathbf{0}_{s\times N} \\ \mathbf{0}_{s\times N} & \boxed{\mathbf{P}} & \mathbf{0}_{s\times N} \\ \mathbf{0}_{s\times N} & \mathbf{0}_{s\times N} & \boxed{\mathbf{P}} \end{array}\right]\left[\begin{array}{c} \boldsymbol{X}[k-1] \\ \boldsymbol{X}[k] \\ \boldsymbol{X}[k+1] \end{array}\right] + \mathbf{E}\,\mathbf{R}\,\boldsymbol{z}[k], \tag{21}$$

Letting f_s denote the sample rate, the data rate of an OFDM system with PTEQ is

$$R(\gamma_0,\ldots,\gamma_{N-1}) = \frac{f_\mathrm{s}}{N+\nu}\sum_{n=0}^{N-1} b(\gamma_n). \tag{27a}$$

The data rate equation for an OFDM system with PTPC is equivalent, but with $\bar{\gamma}_n$ instead of γ_n.

Discrete MultiTone

The data rate of a DMT system with PTEQ is

$$R(\gamma_0,\ldots,\gamma_{N/2}) = \frac{f_\mathrm{s}}{N+\nu}\left(\frac{1}{2}\sum_{n=0}^{1} b(\gamma_{nN/2}) + \sum_{n=1}^{N/2-1} b(\gamma_n)\right). \tag{27b}$$

The data rate equation for a DMT system with PTPC is equivalent, but with $\bar{\gamma}_n$ instead of γ_n. It is noted that a different value for Γ may be required on the DC ($n = 0$) and Nyquist ($n = \frac{N}{2}$) subcarrier, as their transmitted and received symbols are real. Throughout the paper, it is however assumed w.l.o.g. that Γ is equal on all subcarriers.

III. PTEQ Filter Optimization & Resource Allocation

In a system with PTEQ, the power allocation vector $\boldsymbol{S}$ and the PTEQ filter vectors $\{\boldsymbol{v}_0,\ldots,\boldsymbol{v}_{N-1}\}$ can be optimized jointly based on the following rate maximization problem[8]

$$\underset{\substack{\boldsymbol{S}\in\mathbb{R}_+^N \\ \{\boldsymbol{v}_0,\ldots,\boldsymbol{v}_{N-1}\}}}{\text{maximize}} \quad \sum_{n=0}^{N-1}\log_2\left(1+\Gamma^{-1}\,\gamma_n(\boldsymbol{S},\boldsymbol{v}_n)\right) \tag{28a}$$

$$\text{s.t.} \quad \mathbb{E}\left[|x[k']|^2\right] \le P_\mathrm{sample}. \tag{28b}$$

The expected sample power can be calculated as

$$\mathbb{E}\left[|x[k']|^2\right] = \frac{1}{s}\sum_{n=0}^{N-1} S_n\,|\mathrm{col}_n\,\mathbf{T}|^2, \tag{29}$$

where $|\mathrm{col}_n\,\mathbf{T}^\mathrm{CP}|^2 = \frac{s}{N^2}$ for CP-OFDM, and $|\mathrm{col}_n\,\mathbf{T}^\mathrm{ZP}|^2 = \frac{1}{N}$ for ZP-OFDM. All formulas in the rest of this Section will be valid for both CP-OFDM and ZP-OFDM systems with PTEQ.

Discrete MultiTone

Returning to (27b), it is seen that (28a) does not necessarily model the data rate in DMT systems accurately. However, if $S_{n^*} = S_n$, $\forall n$ and $\boldsymbol{h} \in \mathbb{R}^{L+1}$ — as should be the case in DMT systems — then $\gamma_n(\boldsymbol{S},\boldsymbol{v}_n) = \gamma_{n^*}(\boldsymbol{S},\boldsymbol{v}_n^*)$.[9] Therefore, if constraints enforcing $S_{n^*} = S_n$ and $\boldsymbol{v}_{n^*} = \boldsymbol{v}_n^*$, $\forall n$ are added to the optimization problem in (28), then the objective function in (28a) is indeed proportional to the DMT data rate such that the optimization problem in (28) aptly describes the resource allocation problem in a DMT system with PTEQ as well. At the end of Section III-C, it will be highlighted that even without enforcing $S_{n^*} = S_n$ and $\boldsymbol{v}_{n^*} = \boldsymbol{v}_n^*$ explicitly, these constraints will be satisfied automatically with the proposed algorithm.

A. Problem Reformulation

As the SINR of subcarrier n only depends on the PTEQ filter of subcarrier n (i.e. not on the PTEQ filter of other subcarriers), and as $\log_2(1+\bullet)$ is a monotonically increasing function, it is seen that the optimal PTEQ filter $\boldsymbol{v}_n^\star$ should maximize the SINR γ_n for a given $\boldsymbol{S}$, i.e.

$$\boldsymbol{v}_n^\star = \arg\max_{\boldsymbol{v}_n}\{\gamma_n(\boldsymbol{S},\boldsymbol{v}_n)\}. \tag{30}$$

The optimal PTEQ filter $\boldsymbol{v}_n^\star$ can be calculated in closed form as

$$\boldsymbol{v}_n^\star = \boldsymbol{\Psi}_n(\boldsymbol{S})^{-1}\,\boldsymbol{h}_n. \tag{31}$$

with interference-plus-noise covariance matrix $\boldsymbol{\Psi}_n$ defined as

$$\boldsymbol{\Psi}_n(\boldsymbol{S}) \triangleq \sum_{m=0}^{N-1} S_m\,\mathbb{H}_{nm}\,\mathbb{H}_{nm}^\mathcal{H} + \sigma^2\,\underline{\mathbf{R}}_n\,\underline{\mathbf{R}}_n^\mathcal{H}. \tag{32}$$

The same choice for $\boldsymbol{v}_n$ (up to scaling) also minimizes $\mathbb{E}\left[|X_n[k]-\hat{X}_n[k]|^2\right]$ [9]. Moreover, by plugging (31) back into (15), an expression for the achieved SINR is obtained that is only a function of the transmit power vector $\boldsymbol{S}$:

$$\gamma_n(\boldsymbol{S}) \triangleq \gamma_n(\boldsymbol{S},\boldsymbol{v}_n^\star) = S_n\,\boldsymbol{h}_n^\mathcal{H}\,\boldsymbol{\Psi}_n(\boldsymbol{S})^{-1}\,\boldsymbol{h}_n. \tag{33}$$

As such, $\boldsymbol{v}_n$ can effectively be removed from problem (28) leading to the reformulated rate maximization problem

$$\underset{\boldsymbol{S}\in\mathbb{R}_+^N}{\text{maximize}} \quad \sum_{n=0}^{N-1}\log_2\left(1+\Gamma^{-1}\,\gamma_n(\boldsymbol{S})\right) \tag{34a}$$

$$\text{s.t.} \quad \mathbb{E}\left[|x[k']|^2\right] \le P_\mathrm{sample}. \tag{34b}$$

B. Successive Convex Approximation Algorithm

Even though problem (34) is significantly simplified with respect to problem (28), it is still non-convex and closely related to the NP-hard SISO IC sum-rate maximization problem considered in [30].[10] The subsequently developed algorithm will therefore seek to find a stationary point of problem (34),

[8] Some constants have been dropped in order to simplify notation.

[9] From $\underline{\mathbf{R}}_{n^*} = \underline{\mathbf{R}}_n^*$ and $\mathrm{col}_{n^*}(\mathbf{T}) = (\mathrm{col}_n(\mathbf{T}))^*$, it follows that $\boldsymbol{h}_{n^*m^*}[k] = (\boldsymbol{h}_{nm}[k])^*$ and, by extension, $|(\boldsymbol{v}_n^*)^\mathcal{H}\boldsymbol{h}_{n^*m^*}[k]| = |\boldsymbol{v}_n^\mathcal{H}\boldsymbol{h}_{nm}[k]|$.

[10] If $T = 0$ and box constraints of the form $0 \le S_n \le S_n^\mathrm{max}$ are added to problem (34), then the SISO IC sum-rate maximization problem of [30] is obtained. Even then however, (34) need not be NP-hard as the set of all possible SISO IC power channel coefficients $\left|\mathbb{H}_{ij}\right|^2$ may be a strict subset of $\mathbb{R}_+^{N\times N}$ that yields no NP-hard sum-rate maximization problems.

Algorithm 1. Successive Convex Approximation Framework

1: Choose $\boldsymbol{S}[0] \in \mathcal{S}$
2: **for** $t = 0, 1, \ldots$ **do**
3: Construct the surrogate objective function $\tilde{F}(\bullet|\boldsymbol{S}[t])$
4: Solve surrogate problem (36), yielding $\hat{\boldsymbol{S}}$
5: Update $\boldsymbol{S}[t+1] \leftarrow (1-\theta[t]) \cdot \boldsymbol{S}[t] + \theta[t] \cdot \hat{\boldsymbol{S}}$

rather than its global optimum. A successive convex approximation (SCA) algorithm is proposed which, instead of directly tackling the considered non-convex problem

$$\underset{\boldsymbol{S}\in\mathcal{S}}{\text{maximize}} \; F(\boldsymbol{S}), \tag{35}$$

solves a sequence of more tractable surrogate problems

$$\underset{\boldsymbol{S}\in\mathcal{S}}{\text{maximize}} \; \tilde{F}(\boldsymbol{S}|\tilde{\boldsymbol{S}}) \tag{36}$$

wherein the original non-concave objective function is replaced by simpler concave one. A formal description of the considered SCA algorithm is given as Algorithm 1. Proposition 1 provides theoretical convergence conditions.

Proposition 1 (SCA Convergence): If assumptions **P1.a**-**P1.h** are satisfied,[11] and if in addition the step size $\theta[t]$ satisfies

$$\theta[t] \in (0,1] \qquad \sum_t \theta[t] = +\infty \qquad \sum_t \theta[t]^2 < +\infty$$

then either Algorithm 1 converges to a stationary point of problem (35) in a finite number of iterations, or every limit point of the sequence $\{\boldsymbol{S}[t]\}$ (at least one such point exists) is a stationary point of problem (35).

P1.a $\mathcal{S}$ is non-empty, closed, and convex;
P1.b $F \in C^1$ on an open set $\mathcal{V} \supset \mathcal{S}$;
P1.c ∇F is Lipschitz continuous on $\mathcal{S}$;
P1.d F is bounded from above on $\mathcal{S}$;
P1.e $\tilde{F}(\bullet|\tilde{\boldsymbol{S}}) \in C^1$ on an open set $\mathcal{V} \supset \mathcal{S}$, $\forall \tilde{\boldsymbol{S}} \in \mathcal{S}$;
P1.f $\tilde{F}(\bullet|\tilde{\boldsymbol{S}})$ is uniformly strongly concave, $\forall \tilde{\boldsymbol{S}} \in \mathcal{S}$;
P1.g $\nabla F(\tilde{\boldsymbol{S}}) = \nabla \tilde{F}(\bullet|\tilde{\boldsymbol{S}})\big|_{\boldsymbol{S}=\tilde{\boldsymbol{S}}}$, $\forall \tilde{\boldsymbol{S}} \in \mathcal{S}$;
P1.h $\nabla \tilde{F}(\boldsymbol{S}|\bullet)$ is Lipschitz continuous on $\mathcal{S}$ for all $\boldsymbol{S} \in \mathcal{S}$.

Proof: See proof of Theorem 1 in [31]. ∎

Note that line search methods can be used to relax the convergence conditions from Proposition 1 [32]. However, experience has shown that if the surrogate problem is chosen as a suitable approximant of the original optimization problem, an SCA algorithm converges to a sufficiently accurate solution in only a few iterations [31], [33]–[35]. As will be demonstrated in Section V, the same convergence behavior characterizes Algorithm 1 when applied to problem (34) with a surrogate problem that is as proposed in the ensuing paragraph.

As a surrogate to (34), the following problem is proposed:

$$\underset{\boldsymbol{S}\in\mathbb{R}_+^N}{\text{maximize}} \quad \sum_{n=0}^{N-1} \left(\log_2\left(1 + \Gamma^{-1} S_n \, \psi_n(\tilde{\boldsymbol{S}})\right) - S_n \, a_n(\tilde{\boldsymbol{S}}) \right) \tag{37a}$$

$$\text{s.t.} \quad \mathbb{E}\left[|x[k']|^2\right] \leq P_{\text{sample}} \tag{37b}$$

[11] In [31], it is additionally assumed that F is *coercive*, i.e. that $F(\boldsymbol{x}) \to -\infty$ as $\|\boldsymbol{x}\| \to +\infty$, such that the iterates produced by Algorithm 1 are bounded. In the context of problem (34), boundedness of the iterates directly follows from boundedness of the feasible set $\left\{\boldsymbol{S} \in \mathbb{R}_+^N \mid \sum_{n=0}^{N-1} S_n \; |\text{col}_n \, \mathbf{T}|^2 \leq s P_{\text{sample}}\right\}$.

where the functions ψ_n and a_n are defined as

$$\psi_n(\tilde{\boldsymbol{S}}) \triangleq \boldsymbol{h}_n^{\mathcal{H}} \, \boldsymbol{\Psi}_n(\tilde{\boldsymbol{S}})^{-1} \, \boldsymbol{h}_n, \tag{38a}$$

$$a_n(\tilde{\boldsymbol{S}}) \triangleq \sum_{m=0}^{N-1} \frac{\tilde{S}_m/\log(2)}{\Gamma + \gamma_m(\tilde{\boldsymbol{S}})} \cdot \left|\mathbb{H}_{mn}^{\mathcal{H}} \, \boldsymbol{\Psi}_m(\tilde{\boldsymbol{S}})^{-1} \, \boldsymbol{h}_m\right|^2. \tag{38b}$$

The following Proposition and its proof justify this choice for the surrogate problem.

Proposition 2 (SCA Framework Conformity): If $\sigma^2 \, \underline{\mathbf{R}}_n \, \underline{\mathbf{R}}_n^{\mathcal{H}} > \mathbf{0}$ and $|\boldsymbol{h}_n|^2 > 0 \; \forall n$, then problem (34) and its surrogate as in (37) satisfy assumptions **P1.a**-**P1.h** of Proposition 1.

Proof: See Appendix. ∎

Even though $|\boldsymbol{h}_n|^2 > 0$ is required to satisfy conditions **P1.a**-**P1.h**, convergence of Algorithm 1 is still guaranteed when $|\boldsymbol{h}_n|^2 = 0$ for some subcarriers. To see this, note that the optimal power allocation for any subcarrier with $|\boldsymbol{h}_n|^2 = 0$ is $S_n = 0$, which is exactly the value yielded for $\hat{S}_n$ on line 4 of Algorithm 1. By excluding subcarriers n for which $|\boldsymbol{h}_n|^2 = 0$ from the objective of (34) before applying the above convergence analysis, the convergence result can be straightforwardly extended to the case where $|\boldsymbol{h}_n|^2 > 0$ for at least one subcarrier. Moreover, the definition of $\underline{\mathbf{R}}_n$ in (9) implies that condition $\sigma^2 \, \underline{\mathbf{R}}_n \, \underline{\mathbf{R}}_n^{\mathcal{H}} > \mathbf{0}$ is satisfied for both CP-OFDM and ZP-OFDM systems with PTEQ when $\sigma^2 > 0$. It can therefore be concluded that if $|\boldsymbol{h}_n|^2 > 0$ for at least one subcarrier n and $\sigma^2 > 0$, any limit point of Algorithm 1, with the surrogate problem defined as in (37), is a stationary point of problem (34).

C. Solving the Surrogate Problem

The surrogate problem in (37) can be solved by dual decomposition, i.e. by solving the Lagrange dual problem

$$\underset{\lambda\in\mathbb{R}_+}{\text{minimize}} \quad q(\lambda) \triangleq \lambda s P_{\text{sample}} + \sum_{n=0}^{N-1} \max_{S_n \in \mathbb{R}_+} \mathcal{L}_n(S_n, \lambda), \tag{39}$$

where the per-subcarrier Lagrangian $\mathcal{L}_n(\lambda, S_n)$ is defined as

$$\mathcal{L}_n(S_n, \lambda) \triangleq \log_2\left(1 + \Gamma^{-1} S_n \, \psi_n(\tilde{\boldsymbol{S}})\right) - S_n \left(a_n(\tilde{\boldsymbol{S}}) + \lambda \; |\text{col}_n \, \mathbf{T}|^2\right). \tag{40}$$

The Lagrange dual problem in (39) is one-dimensional and convex, such that the optimal Lagrange multiplier $\lambda^\star$ can be obtained using a bisection algorithm. Moreover, strong concavity of $\mathcal{L}_n$ for fixed λ — which follows from strong concavity of the surrogate problem, as proven in Proposition 2 — implies that the solution to problem (37) is given by the maximizer of $\mathcal{L}_n$ at the optimal Lagrange multiplier $\lambda^\star$, and can be calculated analytically as

$$S_i^\star = \left[\frac{1/\log(2)}{a_n(\tilde{\boldsymbol{S}}) + \lambda^\star \; |\text{col}_n \, \mathbf{T}|^2} - \Gamma \, \psi_n(\tilde{\boldsymbol{S}})^{-1}\right]^+. \tag{41}$$

The asymptotic complexity of the above method solving problem (37) is $O(I_{\text{bct}} N)$, where I_{bct} is the expected number of bisection iterations. Constructing the surrogate problem however, which entails evaluating a_n and ψ_n for each $n \in \{0, \ldots, N-1\}$, requires executing $O\left(NT^2(N+T)\right)$ flops. As

N can be large — e.g. $N = 4096$ for the 106b-profile of G.fast [2] — the complexity of the above method is dominated by the complexity of constructing the surrogate problem.

From the proposed SCA algorithm, other low complexity power allocation algorithms can be derived. For example, an iterative water filling (IWF) algorithm [36] can be obtained by defining $a_n(\tilde{\boldsymbol{S}}) = 0$. In addition, a constant offset autonomous spectrum balancing (CO-ASB) algorithm [14], [37] can be obtained by setting $a_n(\tilde{\boldsymbol{S}})$ to a predetermined constant value. Both IWF and CO-ASB can be implemented rather easily by, in each iteration, estimating $\psi_n(\boldsymbol{S})$ $\forall n$, solving the resulting surrogate problem, and applying the resulting $\boldsymbol{S}$ during transmission. The convergence analysis of Algorithm 1 does not apply to IWF and CO-ASB. In Section V, it will however be shown that the IWF algorithm achieves close-to-optimal performance when ISI/ICI is sufficiently suppressed by the PTEQ filter.

Discrete MultiTone

Finally, a comment is due highlighting that the proposed algorithm automatically satisfies $S_{n^*} = S_n$ and $\boldsymbol{w}_{n^*} = \boldsymbol{w}_n^*$ when considering DMT systems. When $\boldsymbol{S}$ is Hermitian symmetric and $\boldsymbol{h}$ is real, it follows from (31) and (32) that $\boldsymbol{w}_{n^*}^\star = (\boldsymbol{w}_n^\star)^*$. Therefore it remains to show that the final $\boldsymbol{S}[k]$ yielded by Algorithm 1 is Hermitian symmetric. When $\boldsymbol{S}$ is Hermitian symmetric and $\boldsymbol{h}$ is real, it additionally follows from (38a) and (38b) that $\psi_{n^*}(\boldsymbol{S}) = \psi_n(\boldsymbol{S})$ and $a_{n^*}(\boldsymbol{S}) = a_n(\boldsymbol{S})$. Consequently, (41) will yield a Hermitian symmetric solution $\boldsymbol{S}^\star$. By using an induction argument, it can then be proven that — provided that $\boldsymbol{S}[0]$ in Algorithm 1 is Hermitian symmetric and $\boldsymbol{h}$ is real — each iterate $\boldsymbol{S}[t]$ produced by Algorithm 1 will be Hermitian symmetric as well.

IV. PTPC Filter Optimization & Resource Allocation

In an OFDM system with PTPC, the power allocation vector $\boldsymbol{S}$ and the PTPC filter vectors $\{\bar{\boldsymbol{v}}_0, \ldots, \bar{\boldsymbol{v}}_N\}$ can be optimized jointly based on the following rate optimization problem.

$$\underset{\substack{\bar{\boldsymbol{S}} \in \mathbb{R}_+^N \\ \{\bar{\boldsymbol{v}}_0, \ldots, \bar{\boldsymbol{v}}_{N-1}\}}}{\text{maximize}} \quad \sum_{i=0}^{N-1} \log_2\left(1 + \Gamma^{-1}\, \bar{\gamma}_n(\bar{\boldsymbol{S}}, \bar{\boldsymbol{v}}_1, \ldots, \bar{\boldsymbol{v}}_N)\right) \tag{42a}$$

$$\text{s.t.} \quad \mathbb{E}\left[|x[k']|^2\right] \leq P_{\text{sample}} \tag{42b}$$

In (42b), the expected sample power is

$$\mathbb{E}\left[|x[k']|^2\right] = s^{-1} \sum_{n=0}^{N-1} \bar{S}_n \, |\underline{\mathbf{T}}_n \, \bar{\boldsymbol{v}}_n|^2 \,. \tag{43}$$

At first glance, the optimization problem in (42) seems more involved than the one in (28). In particular, eliminating $\bar{\boldsymbol{v}}_n$ — as was done for the PTEQ problem in Section III — is not straightforward because the SINR of subcarrier n now depends on the PTPC filter of all subcarriers (i.e. not only the PTPC filter of subcarrier n). Nonetheless, Sections IV-A to IV-C will demonstrate that problem (28) and problem (42) are equivalent.

A. Dual System with PTEQ

The duality result will be established between the system with PTPC, as described by (21), and its dual system, which is characterized by the following input-output equation:

$$\hat{X}_n[k] = \bar{\boldsymbol{v}}_n^{\mathcal{H}} \underline{\mathbf{T}}_n^{\mathcal{H}} \sum_{l=-1}^{1} (\bar{\mathbf{H}}_\delta[-l])^{\mathcal{H}} \mathbf{R}^{\mathcal{H}} \boldsymbol{X}[k+l] + N\, \bar{\boldsymbol{v}}_n^{\mathcal{H}} \underline{\mathbf{T}}_n^{\mathcal{H}} \tilde{\boldsymbol{z}}[k]. \tag{44}$$

The channel matrix in (44), when written as

$$\left[\; (\bar{\mathbf{H}}_\delta[1])^{\mathcal{H}} \;\middle|\; (\bar{\mathbf{H}}_\delta[0])^{\mathcal{H}} \;\middle|\; (\bar{\mathbf{H}}_\delta[-1])^{\mathcal{H}} \;\right], \tag{45}$$

is seen to have a Toeplitz structure as well. This Toeplitz structure allows the channel model in (44) to be rewritten as in (46a) at the top of the next page, where $\mathbf{O}_5$ has dimensions $(s+T)\times(s-T-\delta)$, $\mathbf{O}_6$ has dimensions $(s+T)\times(s-L+\delta)$, and $\mathbf{J}_{L+1}$ is an $(L+1)\times(L+1)$ exchange matrix with $[\mathbf{J}_{L+1}]_{n,m} = 1$ for $m = L+1-n$ and $[\mathbf{J}_{L+1}]_{n,m} = 0$ otherwise. Before stating the duality result that connects the system described by (44) and (46a) to the OFDM system with PTPC, it will be established that the system characterized by input-output equations (44) and (46a) correspond to an OFDM system with PTEQ.

1) Dual of the CP-OFDM System with PTPC

First, the case is considered where the transmit and receive matrices in (44) and (46a) correspond to a CP-OFDM system. The identity $N\,\mathcal{I}_N = \mathcal{F}_N^{\mathcal{H}}$ implies that the following hold:

$$\begin{bmatrix} (\mathbf{R}^{\text{CP}})^{\mathcal{H}} & & \\ & (\mathbf{R}^{\text{CP}})^{\mathcal{H}} & \\ & & (\mathbf{R}^{\text{CP}})^{\mathcal{H}} \end{bmatrix} = N\, \boldsymbol{\Theta}_{3s}^{\nu} \begin{bmatrix} \mathbf{T}^{\text{ZP}} & & \\ & \mathbf{T}^{\text{ZP}} & \\ & & \mathbf{T}^{\text{ZP}} \end{bmatrix} \tag{47a}$$

$$(\underline{\mathbf{T}}_n^{\text{CP}})^{\mathcal{H}} = \frac{1}{N}\, \underline{\mathbf{R}}_n^{\text{ZP}} \tag{47b}$$

where $\boldsymbol{\Theta}_a^b$ shifts the rows of $\mathbf{T}^{\text{ZP}}$ down by ν positions, and is defined as

$$\boldsymbol{\Theta}_a^b \triangleq \left[\; \begin{array}{c} \mathbf{0} \\ \mathbf{I}_{a-b} \end{array} \;\middle|\; \mathbf{0}_{b\times a} \;\right]. \tag{48}$$

After substituting (47) into (46a), the Toeplitz channel matrix from (46a) is right multiplied by $\boldsymbol{\Theta}_{3s}^{\nu}$ which shifts its columns to the left by ν positions. As the last ν rows of $\mathbf{T}^{\text{ZP}}$ contain only zeros, the last ν columns of the shifted channel matrix can be freely modified such that the result is again a Toeplitz matrix. This yields the input-output equation in (46b) where the dimensions of $\mathbf{O}_7$ and $\mathbf{O}_8$ are respectively $(s+T)\times(s-T-\nu-\delta)$ and $(s+T)\times(s-L+\nu+\delta)$. It is noted that, similarly to how (46b) was obtained from (46a), (46a) can also be obtained from (46b). Moreover, the superscript "DE" — which stands for "dual symbol extension" — indicates that the transmit and receive matrices in (46b) correspond to a ZP-OFDM system, whereas the transmit and receive matrices in (44) corresponded to a CP-OFDM system.

The channel model in (44) thus describes a ZP-OFDM system with PTEQ as in (12), but with a time-reversed CIR and where $\delta = L - \nu$ aligns all signals such that $y_0[k]$ is the first sample that has a contribution from $\boldsymbol{X}[k]$. Also, it is noted that the PTEQ filters in the system corresponding to (44) have their coefficients in reversed order when compared

$$\hat{X}_n[k] = \bar{\boldsymbol{v}}_n^{\mathcal{H}} \underline{\mathbf{T}}_n^{\mathcal{H}} \left[\begin{array}{c|ccc|c} \mathbf{O}_5 & \boxed{\boldsymbol{h}^* \mathbf{J}_{L+1}} & 0 & \cdots & \\ & 0 & \ddots & \ddots & \mathbf{O}_6 \\ & \vdots & \ddots & \boxed{\boldsymbol{h}^* \mathbf{J}_{L+1}} & \end{array}\right] \left[\begin{array}{ccc} \mathbf{R}^{\mathcal{H}} & & \\ & \mathbf{R}^{\mathcal{H}} & \\ & & \mathbf{R}^{\mathcal{H}} \end{array}\right] \left[\begin{array}{c} \boldsymbol{X}[k-1] \\ \boldsymbol{X}[k] \\ \boldsymbol{X}[k+1] \end{array}\right] + N\, \bar{\boldsymbol{v}}_n^{\mathcal{H}} \underline{\mathbf{T}}_n^{\mathcal{H}} \tilde{\boldsymbol{z}}[k] \tag{46a}$$

$$\hat{X}_n[k] = \bar{\boldsymbol{v}}_n^{\mathcal{H}} \underline{\mathbf{R}}_n^{\mathrm{DE}} \left[\begin{array}{c|ccc|c} \mathbf{O}_7 & \boxed{\boldsymbol{h}^* \mathbf{J}_{L+1}} & 0 & \cdots & \\ & 0 & \ddots & \ddots & \mathbf{O}_8 \\ & \vdots & \ddots & \boxed{\boldsymbol{h}^* \mathbf{J}_{L+1}} & \end{array}\right] \left[\begin{array}{ccc} \mathbf{T}^{\mathrm{DE}} & & \\ & \mathbf{T}^{\mathrm{DE}} & \\ & & \mathbf{T}^{\mathrm{DE}} \end{array}\right] \left[\begin{array}{c} \boldsymbol{X}[k-1] \\ \boldsymbol{X}[k] \\ \boldsymbol{X}[k+1] \end{array}\right] + \bar{\boldsymbol{v}}_n^{\mathcal{H}} \underline{\mathbf{R}}_n^{\mathrm{DE}} \tilde{\boldsymbol{z}}[k] \tag{46b}$$

to the PTPC filters in the original system from (21). For a CP-OFDM system with PTPC, the system characterized by (44) will be referred to as the *dual ZP-OFDM system with PTEQ*.

2) Dual of the ZP-OFDM System with PTPC

Second, the case is considered where the transmit and receive matrices in (44) and (46a) correspond to a ZP-OFDM system. The identity $N\,\mathcal{I}_N = \mathcal{F}_N^{\mathcal{H}}$ implies that the following hold.

$$\left[\begin{array}{ccc} (\mathbf{R}^{\mathrm{ZP}})^{\mathcal{H}} & & \\ & (\mathbf{R}^{\mathrm{ZP}})^{\mathcal{H}} & \\ & & (\mathbf{R}^{\mathrm{ZP}})^{\mathcal{H}} \end{array}\right] = N \left[\begin{array}{ccc} \mathbf{T}^{\mathrm{CP}} & & \\ & \mathbf{T}^{\mathrm{CP}} & \\ & & \mathbf{T}^{\mathrm{CP}} \end{array}\right] \tag{49a}$$

$$(\underline{\mathbf{T}}_n^{\mathrm{ZP}})^{\mathcal{H}} = \frac{1}{N}\, \underline{\mathbf{R}}_n^{\mathrm{CP}}\, \boldsymbol{\Theta}_{s+T}^{\nu} \tag{49b}$$

After substituting (49) into (46a), the Toeplitz channel matrix from (46a) is left multiplied by $\boldsymbol{\Theta}_{s+T}^{\nu}$ which shifts its rows down by ν positions. As the first ν columns of $\mathbf{R}^{\mathrm{CP}}$ contain only zeros, the first ν rows of the shifted channel matrix can be freely modified such that the result is again a Toeplitz matrix. This yields the input-output equation in (46b), where the dimensions of $\mathbf{O}_7$ and $\mathbf{O}_8$ are the same as before. It is noted that, similarly to how (46b) was obtained from (46a), (46a) can also be obtained from (46b). Moreover, the superscript "DE" indicates that the transmit and receive matrices in (46b) correspond to a CP-OFDM, whereas the transmit and receive matrices in (44) corresponded to a ZP-OFDM system.

The channel model in (44) thus describes a CP-OFDM system with PTEQ as in (12), but with a time-reversed CIR and where $\delta = L - \nu$ aligns all signals such that $y_0[k]$ is the first sample that has a contribution from $\boldsymbol{X}[k]$. As before, it is noted that the PTEQ filters in the system corresponding to (44) have their coefficients in reversed order when compared to the PTPC filters in the original system from (21). For a ZP-OFDM system with PTPC, the system characterized by (44) will be referred to as the *dual CP-OFDM system with PTEQ*.

B. PTEQ-PTPC Duality

As a final step before deriving the duality result, an SINR expression is established for the dual system with PTEQ. It is noted that the SINR expression from (15) is still valid — provided that the correct channel matrix is employed. However, a slightly different SINR expression will be derived here, which will yield a clearer exposition of the duality result in the ensuing paragraphs. It is once more assumed that $\mathbb{E}\left[|z[k']|^2\right] = \sigma^2$, and that $\mathbb{E}\left[\boldsymbol{X}[k]\,\boldsymbol{X}[l]^{\mathcal{H}}\right]$ conforms to (1). Then, using the definitions of the residual channel vectors $\bar{\boldsymbol{h}}_{ij}[k]$ and matrices $\bar{\mathbb{H}}_{ij}$ as in (24), the following SINR expression is obtained for subcarrier n of the dual system with PTEQ:

$$\bar{\bar{\gamma}}_n(\boldsymbol{S}, \bar{\boldsymbol{v}}_n) = \frac{S_n \left|\bar{\boldsymbol{v}}_n^{\mathcal{H}} \bar{\boldsymbol{h}}_n\right|^2}{\sum_{m=0}^{N-1} S_m \left|\bar{\boldsymbol{v}}_n^{\mathcal{H}} \bar{\mathbb{H}}_{mn}\right|^2 + N^2\, \sigma^2\, |\underline{\mathbf{T}}_n\, \bar{\boldsymbol{v}}_n|^2}. \tag{50}$$

A duality result will now be established between the system with PTPC, which is characterized by (21), and the dual system with PTEQ characterized by (44). The duality statement and its derivation are based on [19]–[21], [35].

Proposition 3 (PTEQ-PTPC duality): Choose any set of PTPC vectors $[\bar{\boldsymbol{v}}_0, \ldots, \bar{\boldsymbol{v}}_{N-1}] \in \mathbb{C}^{(T+1)\times N}$. If $0 < \sigma^2$ and $\bar{\boldsymbol{v}}_n \neq \mathbf{0}_{(T+1)\times 1}$ $\forall n$, then the following statements hold.

P3.a For each dual power vector $\boldsymbol{S} \in \mathbb{R}_+^N$, a corresponding power vector $\bar{\boldsymbol{S}} \in \mathbb{R}_+^N$ exists such that equalities (51a) and (51b) are satisfied.

P3.b The converse is also true, i.e. for each power vector $\bar{\boldsymbol{S}} \in \mathbb{R}_+^N$, a dual power vector $\boldsymbol{S} \in \mathbb{R}_+^N$ exists such that equalities (51a) and (51b) are satisfied.

$$\bar{\gamma}_n(\bar{\boldsymbol{S}}, \bar{\boldsymbol{v}}_0, \ldots, \bar{\boldsymbol{v}}_{N-1}) = \bar{\bar{\gamma}}_n\big(\boldsymbol{S}, \bar{\boldsymbol{v}}_n\big), \quad \forall n \tag{51a}$$

$$\frac{1}{s}\sum_{n=0}^{N-1} \bar{S}_n\, |\underline{\mathbf{T}}_n\, \bar{\boldsymbol{v}}_n|^2 = \frac{1}{s}\sum_{n=0}^{N-1} S_n\, |\mathrm{col}_n\, \mathbf{T}^{\mathrm{DE}}|^2 \tag{51b}$$

Proof: Only **P3.a** will be proven explicitly; the proof of **P3.b** is analogous.

Following the reasoning in [21], the proof of **P3.a** is by construction of $\bar{\boldsymbol{S}}$ from $\boldsymbol{S}$. Equation (52) at the top of the next page reveals that the following system of equations can be obtained from and — given that $0 < \sigma^2$ and $0 < \left|\underline{\mathbf{T}}_n\, \bar{\boldsymbol{v}}_n\right|^2$ $\forall n$ — is equivalent to (51a):

$$\mathbf{Z}\,\bar{\boldsymbol{S}} = \sigma^2 \left[\begin{array}{c} |\mathrm{row}_0\, \mathbf{R}|^2 \\ \vdots \\ |\mathrm{row}_{N-1}\, \mathbf{R}|^2 \end{array}\right] \circ \boldsymbol{S} \tag{53a}$$

where

$$[\mathbf{Z}]_{n,m} \triangleq \left\{\begin{array}{ll} \sum_{\substack{o=0 \\ o\neq n}}^{N-1} S_o \left|\bar{\boldsymbol{v}}_n^{\mathcal{H}} \bar{\mathbb{H}}_{on}\right|^2 + N^2\sigma^2\, |\underline{\mathbf{T}}_n\, \bar{\boldsymbol{v}}_n|^2 & \text{if } n = m \\ -S_n \left|\bar{\boldsymbol{v}}_m^{\mathcal{H}} \bar{\mathbb{H}}_{nm}\right|^2 & \text{if } n \neq m \end{array}\right. . \tag{53b}$$

$$\bar{S}_n \cancel{\left|\bar{\boldsymbol{v}}_n^{\mathcal{H}} \bar{\boldsymbol{h}}_n\right|^2} \left(\cancel{S_n \left|\bar{\boldsymbol{v}}_n^{\mathcal{H}} \bar{\mathbb{H}}_{nn}\right|^2} + \sum_{\substack{m=0 \\ m\neq n}}^{N-1} S_m \left|\bar{\boldsymbol{v}}_n^{\mathcal{H}} \bar{\mathbb{H}}_{mn}\right|^2 + N^2\sigma^2 \left|\underline{\mathbf{T}}_n \bar{\boldsymbol{v}}_n\right|^2 \right) = S_n \cancel{\left|\bar{\boldsymbol{v}}_n^{\mathcal{H}} \bar{\boldsymbol{h}}_n\right|^2} \left(\cancel{\bar{S}_n \left|\bar{\boldsymbol{v}}_n^{\mathcal{H}} \bar{\mathbb{H}}_{nn}\right|^2} + \sum_{\substack{m=0 \\ m\neq n}}^{N-1} \bar{S}_m \left|\bar{\boldsymbol{v}}_m^{\mathcal{H}} \bar{\mathbb{H}}_{nm}\right|^2 + \sigma^2 \left|\text{row}_n \mathbf{R}\right|^2 \right) \tag{52}$$

The matrix $\mathbf{Z}$ is real-valued, has positive diagonal elements and non-positive off-diagonal elements, and is column diagonally dominant. Therefore, $\mathbf{Z}$ is an M-matrix [21]. As M-matrices are inverse positive, it is concluded that for each $\boldsymbol{S} \in \mathbb{R}_+^N$, solving (53) yields an $\bar{\boldsymbol{S}} \in \mathbb{R}_+^N$ for which (51a) is satisfied. By summing all rows of (53), the following equality is obtained.

$$\sum_{n=0}^{N-1} N^2 \bar{S}_n \left|\underline{\mathbf{T}}_n \bar{\boldsymbol{v}}_n\right|^2 = \sum_{n=0}^{N-1} S_n \left|\text{row}_n \mathbf{R}\right|^2$$

After substitution of $|\text{row}_n \mathbf{R}|^2$ with $N^2 \left|\text{col}_n \mathbf{T}^{\text{DE}}\right|^2$, it is seen that the obtained $\bar{\boldsymbol{S}}$ satisfies (51b) as well. ∎

Proposition 3 shows that — if the PTPC vectors $\bar{\boldsymbol{v}}_n$ satisfy some assumption — any feasible resource allocation for the dual ZP/CP-OFDM system with PTEQ that is described by (46b) has a corresponding feasible resource allocation for the CP/ZP-OFDM system with PTPC that achieves the same SINR on all subcarriers as well as the same time-domain sample power $\mathbb{E}\left[|x[k']|^2\right]$, and vice versa. The following Corollary relaxes the assumptions on the PTPC vectors a bit further, and will be required to prove Proposition 6 in Section IV-C.

Corollary 4: **P3.b** also holds when $\bar{\boldsymbol{v}}_n = \mathbf{0}_{(T+1)\times 1}$ for any n.

Proof: See proof of Corollary 2 in [35]. ∎

Discrete MultiTone

When a DMT system is considered rather than an OFDM system, one should additionally assert that a feasible DMT PTEQ resource allocation always has a corresponding feasible DMT PTPC resource allocation and vice versa. The required result is provided by Proposition 5.

Proposition 5 (PTEQ-PTPC duality — DMT): If $\bar{\boldsymbol{v}}_{n^*} = \bar{\boldsymbol{v}}_n^*$ $\forall n$ and $\boldsymbol{h} \in \mathbb{R}^{L+1}$, then Proposition 3 also holds when both $\bar{\boldsymbol{S}}$ and $\boldsymbol{S}$ are confined to the set $\{\boldsymbol{S} \in \mathbb{R}_+^N \mid S_{n^*} = S_n, \forall n\}$.

Proof: As before, only **P3.a** will be proven explicitly. The proof of **P3.b** is analogous.

Proposition 5 is proven by showing that, if its assumptions are satisfied and in addition $\boldsymbol{S}$ is Hermitian symmetric, solving (53) yields a Hermitian symmetric $\bar{\boldsymbol{S}}$. The definitions of $\mathbf{R}^{\text{CP}}$, $\mathbf{R}^{\text{ZP}}$, $\underline{\mathbf{T}}_n^{\text{CP}}$ and $\underline{\mathbf{T}}_n^{\text{ZP}}$ imply that $\text{row}_{n^*}(\mathbf{R}) = (\text{row}_n(\mathbf{R}))^*$ and $\underline{\mathbf{T}}_{n^*} = \underline{\mathbf{T}}_n^*$. As $\boldsymbol{h} \in \mathbb{R}^{L+1}$, it follows that $\bar{\mathbb{H}}_{n^*m^*} = (\bar{\mathbb{H}}_{nm})^*$. Keeping in mind that both $S_n = S_{n^*}$ and $\bar{\boldsymbol{v}}_{n^*} = \bar{\boldsymbol{v}}_n^*$, it is then seen that $\mathbf{Z}$ in (53) satisfies $[\mathbf{Z}]_{n,m} = [\mathbf{Z}]_{n^*,m^*}$ $\forall i, j$. This fact can also be expressed as

$$\mathbf{Z} = \mathbf{\Pi}\,\mathbf{Z}\,\mathbf{\Pi}, \tag{54}$$

where $\mathbf{\Pi} \triangleq \left[\boldsymbol{e}_{0^*}, \ldots, \boldsymbol{e}_{(N-1)^*}\right]$ is a permutation matrix, with $\boldsymbol{e}_n$ the $(n+1)$-th vector in the standard basis of $\mathbb{R}^N$. As $\mathbf{\Pi} = \mathbf{\Pi}^{-1}$, the solution to (53) satisfies

$$\bar{\boldsymbol{S}} \propto \mathbf{Z}^{-1}\,\boldsymbol{S} = \mathbf{\Pi}\,\mathbf{Z}^{-1}\,\mathbf{\Pi}\,\boldsymbol{S}. \tag{55}$$

Hermitian symmetry of $\bar{\boldsymbol{S}}$ then directly follows from the Hermitian symmetry of $\boldsymbol{S}$, i.e. from the fact that $\boldsymbol{S} = \mathbf{\Pi}\,\boldsymbol{S}$. ∎

C. PTPC Filter Optimization & Resource Allocation based on PTEQ-PTPC Duality

Finally, the results from Section IV-B can be used to show that problem (28) and problem (42) are equivalent.

Proposition 6 (PTEQ-PTPC equivalence): Consider the resource allocation problem for the dual system with PTEQ as in (44), which is defined as

$$\underset{\substack{\boldsymbol{S}\in\mathbb{R}_+^N \\ \{\bar{\boldsymbol{v}}_0,\ldots,\bar{\boldsymbol{v}}_{N-1}\}}}{\text{maximize}} \quad \sum_{n=0}^{N-1} \log_2\left(1 + \Gamma^{-1}\,\bar{\bar{\gamma}}_n(\boldsymbol{S}, \bar{\boldsymbol{v}}_n)\right) \tag{56a}$$

$$\text{s.t.} \quad \mathbb{E}\left[|x[k']|^2\right] \leq P_{\text{sample}}. \tag{56b}$$

The solution to problem (56), when transformed to the PTPC domain by solving (53), is the solution to the PTPC problem as in (42).

Proof: The Proposition is proven by contradiction. Assume w.l.o.g. that a solution to problem (56) exists with $\bar{\boldsymbol{v}}_n \neq \mathbf{0}_{(T+1)\times 1}$ $\forall n$. If Proposition 6 were false, a solution to problem (42) would exist achieving a higher objective function value than the transformed solution of (56). Corollary 4 would then imply that a PTEQ resource allocation exists achieving a value for the objective function in (56) that is higher than the value achieved by the solution to (56), which is a contradiction. ∎

Proposition 6 thus yields a method for PTPC resource allocation: find a stationary point of problem (56) using the PTEQ resource allocation algorithm described in Section III, and transform the obtained solution to the PTPC domain by solving the system of equations in (53). Even if the PTEQ resource allocation algorithm is unable to find the globally optimal solution to problem (56), Proposition 3 implies that the transformed solution will always be a feasible PTPC resource allocation.

Finally, it is observed that the results in Section IV-B also establish a duality between ZP/CP-OFDM systems with TEQ and CP/ZP-OFDM system with TPC. This is true as the subset of dual PTEQ filters that can be implemented as a dual TEQ filter is equivalent to the subset of PTPC filters that can be implemented as a TPC filter. The duality result in Section IV-B can thus also be employed to design a TPC filter from a TEQ filter.

V. Simulation Results

The resource allocation algorithms are assessed in the context of single-user long-reach G.fast systems. As G.fast

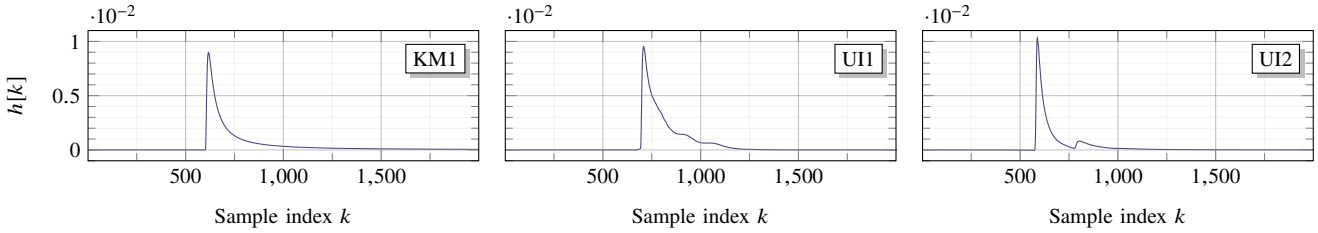

Fig. 3. The three impulse responses (IRs) that are considered in the simulations. The IR labeled "KM1" was synthesized using the KM1 model with k-parameters corresponding to a homogeneous and perfectly terminated Cat5 cable [38, Table II]. The IRs labeled "UI1" and "UI2" were obtained by measurement of the transfer function of twisted-pair cables belonging to two different undisclosed Internet service providers. Both measured IRs were artificially extended to 600 m.

TABLE I
SIMULATION PARAMETERS

Parameter	Value	Parameter	Value
P_{tot}	8 dBm	f_{s}	212 MHz
N	4096	Γ	9.45 dB
σ_f^2	−145 dBm/Hz		

employs CP-DMT only, this section evaluates the performance of both a CP-DMT system with PTEQ and a CP-DMT system with PTPC. Three long-reach DSL scenarios are considered, with CIRs — which are given in Fig. 3 — corresponding to twisted pair cables of length 600 m. This line length is justified by the fact that the purpose of the LR extension of G.fast [3]–[7] is to enable the use of G.fast on lines that have lengths well in excess of the currently imposed 300 m limit. Two CIRs are derived from measured frequency responses, the other is synthesized using the KM1 model [38]. Both measured IRs are artificially extended to 600 m using the following equation:

$$H_1(f) = (H_0(f))^{\frac{l_1}{l_0}}, \tag{57}$$

where l_0 is the original length and l_1 is the target length.

The simulation parameters are chosen conform with the 106b-profile of the G.fast standard [2], and can be found in Table I. The G.fast aggregate transmit power (ATP) constraint is often formulated as

$$\frac{f_{\text{s}}}{N} \sum_{n=1}^{N/2-1} S_n \leq P_{\text{tot}}. \tag{58}$$

G.fast employs CP-DMT, with subcarriers corresponding to the DC ($n = 0$) and Nyquist ($n = \frac{N}{2}$) frequencies carrying no information. As such, it is seen from (28b) and (29) that the ATP constraint as in (58) can equivalently be enforced in a CP-OFDM system by choosing the maximum sample power as

$$P_{\text{sample}} = \frac{2P_{\text{tot}}}{Nf_{\text{s}}}. \tag{59}$$

The value of P_{sample} is calculated as in (59) for the CP-DMT system both with PTEQ and with PTPC. As such, the average power in the time domain is equal in both systems. Care should also be taken when selecting the time-domain noise power σ^2, as one would typically only define the frequency-domain noise power σ_f^2 in DSL simulations. With the DFT operation in the DMT demodulation defined as in (3), the relation between the two is as follows.

$$\sigma_f^2 = N\sigma^2 \tag{60}$$

As the LR extension of G.fast is expected to not use the first 18 subcarriers, these are considered to be inactive — i.e. $S_n = 0\ \forall n \in \{0, \ldots, 17\}$.[12] No spectral mask constraints are considered, as enforcing them in the CP-DMT system with PTPC is not straightforward when the PTPC filter and resource allocation are optimized based on the developed PTEQ-PTPC duality.

A. PTEQ and PTPC performance

Fig. 4 presents the data rate achieved by the considered CP-DMT systems with PTEQ and PTPC for delays δ ranging from $\delta_0 - 200$ to $\delta_0 + 100$, where the delay sweep is executed with a 10 sample granularity. Delays are relative to a reference delay δ_0, which is chosen by maximizing the energy in $\left[h[\delta_0], \ldots, h[\delta_0 + \nu]\right]$ as in [9]. The considered CP length is $\nu = 320$, and PTEQ/PTPC filter order is chosen from $T \in \{0, 1, 7\}$. The resource allocation is executed either with the IWF algorithm, or with the SCA algorithm. Both algorithms are stopped after 10 iterations.

In addition, Fig. 4 also presents the data rate achieved by CP-DMT systems with TEQ and TPC filters. Results are given for the same δ-range, T-values and CP length as were considered for the CP-DMT systems with PTEQ and PTPC. The TEQ filter coefficients are determined using the method described in [39]. After determining the TEQ filter coefficients, the power allocation vector is optimized using an adapted version of either the SCA or the IWF method from Section III. Three adaptations are needed in these methods in order to make them compatible with an additional TEQ filter: 1) the PTEQ filter order is set to $T = 0$, regardless of the TEQ filter order; 2) the CIR are convolved with the TEQ-filter; and 3) the time-domain noise covariance matrix is adapted such that it accounts for the effect of the TEQ. The TPC system is designed by applying the same procedure to the dual ZP-DMT system, and by subsequently employing the duality

[12] It is readily shown that the duality result in Proposition 3 also holds when both $\bar{\boldsymbol{S}}$ and $\boldsymbol{S}$ are confined to the set $\{\boldsymbol{S} \in \mathbb{R}_+^N \mid S_n = 0,\ \forall n \in \mathcal{N}\}$ where $\mathcal{N} \subseteq \{0, \ldots, N-1\}$. In the system with PTPC, one can thus enforce the inactivity constraint by enforcing it in the dual system with PTEQ.

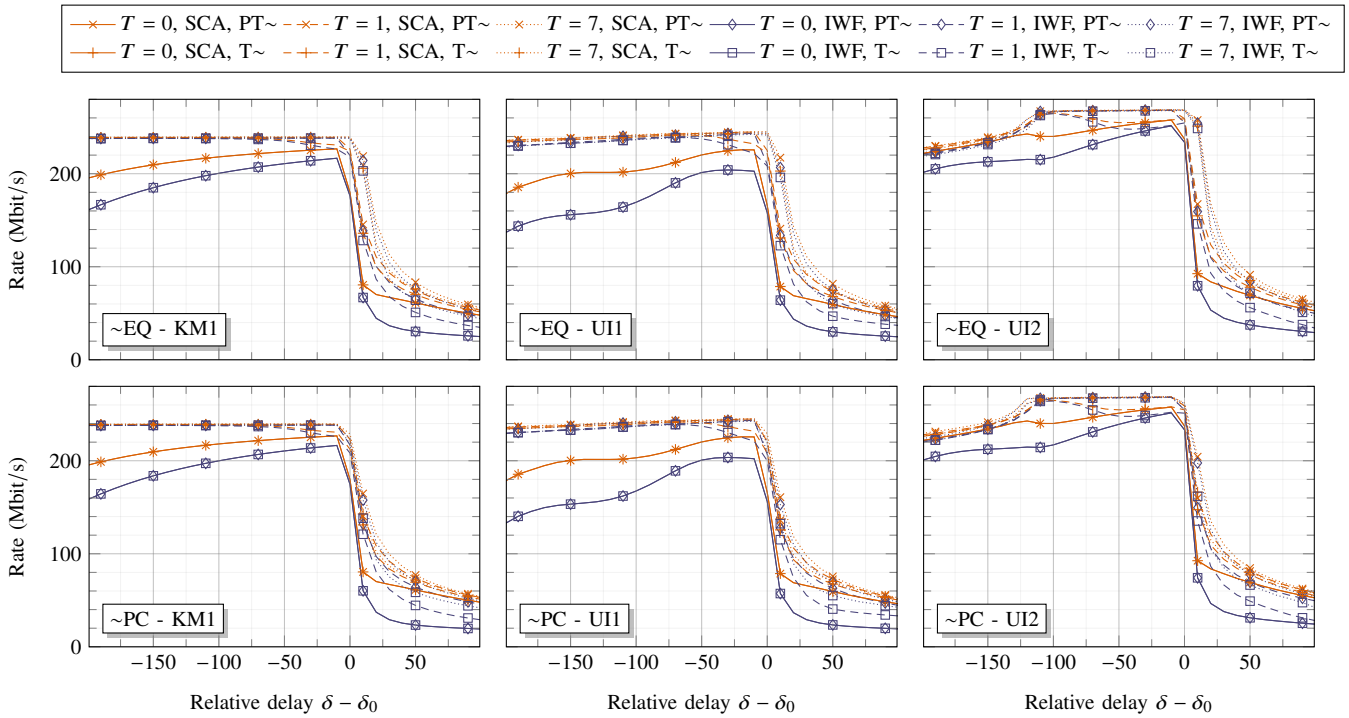

Fig. 4. Data rate achieved by the considered CP-DMT systems with TEQ, PTEQ, TPC, and PTPC after 10 iterations of either the SCA or the IWF algorithm. Delays are relative to a reference delay δ_0, which is chosen by maximizing the energy in $\left[h[\delta_0], \ldots, h[\delta_0+\nu]\right]$ as in [9]. The granularity of the delay sweep is 10 samples. The considered CP length is $\nu = 320$.

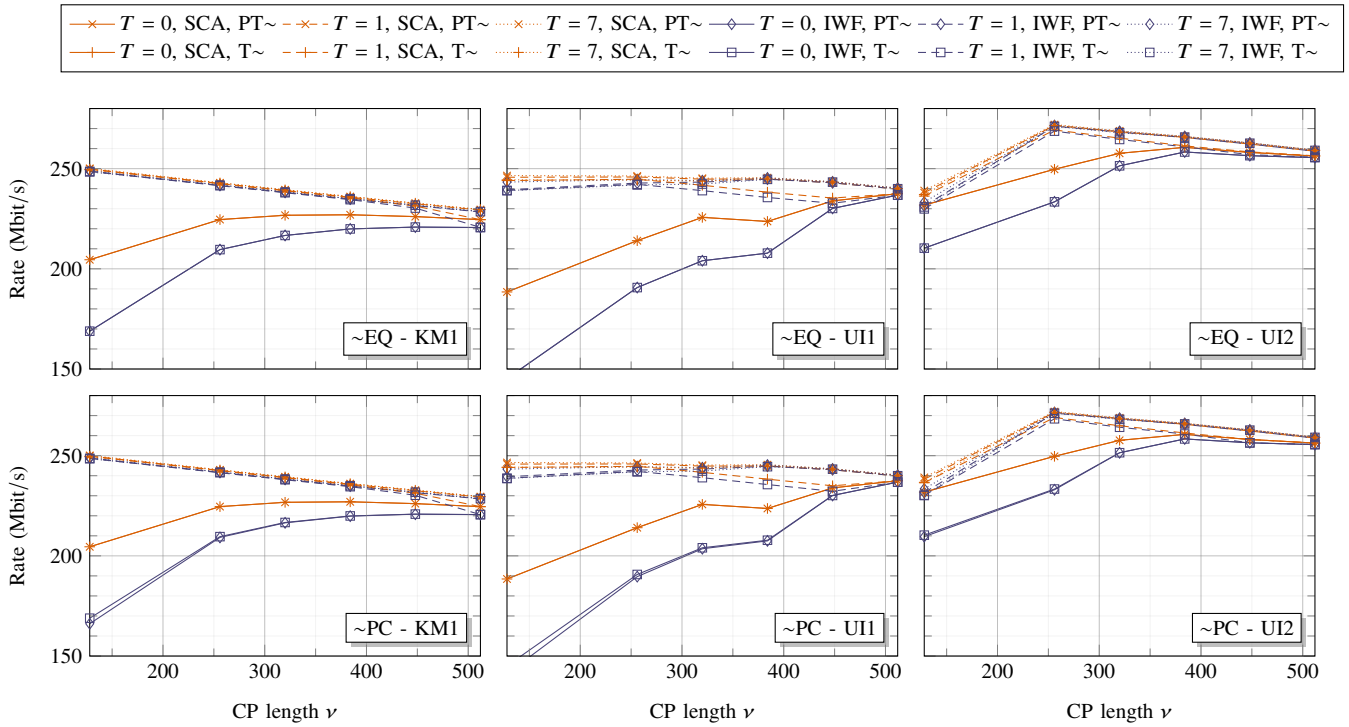

Fig. 5. Data rate achieved by the considered CP-DMT systems with TEQ, PTEQ, TPC, and PTPC for different CP lengths. The data points correspond to the maximum data rates that are achieved when sweeping the delay δ from $\delta_0 - 200$ to $\delta_0 + 100$ with a granularity of 10 samples, as in Fig. 4.

result in Section IV-B to obtain the corresponding TPC filter coefficients and power allocation vector.

Fig. 5 presents the data rate achieved by the considered CP-DMT systems with TEQ, PTEQ, TPC, and PTPC for different CP lengths. For each CP length ν, the data points in Fig. 5 correspond to the maximum data rates that are achieved for a delay sweep as presented in Fig. 4.

A first observation that can be made from Fig. 4 and Fig. 5 is that, even for PTEQ/PTPC with $T = 0$ (which corresponds to merely FEQ), careful design of the transmit PSDs can lead to data rates that form an interesting middle ground between true PTEQ/PTPC with $T > 0$, and ISI/ICI-unaware resource allocation. The advantage here, of course, would be that this increase in performance is achieved without the additional system and computational complexity incurred by true PTEQ/PTPC with $T > 0$.

A second observation is that the results obtained for the CP-DMT system with TEQ or PTEQ and those obtained for the CP-DMT system with TPC or PTPC are nearly indistinguishable. As such, TPC and PTPC may be an interesting alternative channel shortening strategy in scenarios where implementing TEQ or PTEQ is either difficult or costly. For instance, in downstream DSL systems, TPC and PTPC enable the implementation of channel shortening without replacing the customer premises equipment. It is noted that this similar performance may be contingent on the assumption of i.i.d. time-domain noise, as it is expected that TEQ and PTEQ can exploit a correlation between noise samples better than TPC and PTPC. While certainly possible, extending the models and algorithms in this paper to include colored noise would further obfuscate the derivations, and is therefore considered to be out-of-scope.

Finally, it is observed in Fig. 5 that — even in a single user system — performance improvements can be obtained by reducing the CP length and employing a short channel shortening filter.

B. SCA convergence

Fig. 6 illustrates the convergence behavior of the SCA algorithm. It shows the distribution of the distance to optimal rate after each iteration t, i.e. the relative difference between the data rate after iteration t and the data rate after iteration 350. The results are obtained by tracking the achieved data rate during all runs of the SCA algorithm that are used to obtain results of the systems with PTPC in Section V-A.

Fig. 6 confirms that the SCA algorithm yields no significant further data rate improvement after the first 20 iterations. However, it does not confirm that the obtained solution is anywhere near a stationary point of problem (56). In order to do so, Fig. 7 additionally illustrates the distribution of the KKT error function ϵ_t as defined in [40, Eq. 9] after each iteration. It is noted that ϵ_t does not necessarily converge to zero [40] for any sequence approaching a KKT point; its definition requires some tweaking before being applicable as a termination criterion for the SCA algorithm. However, the

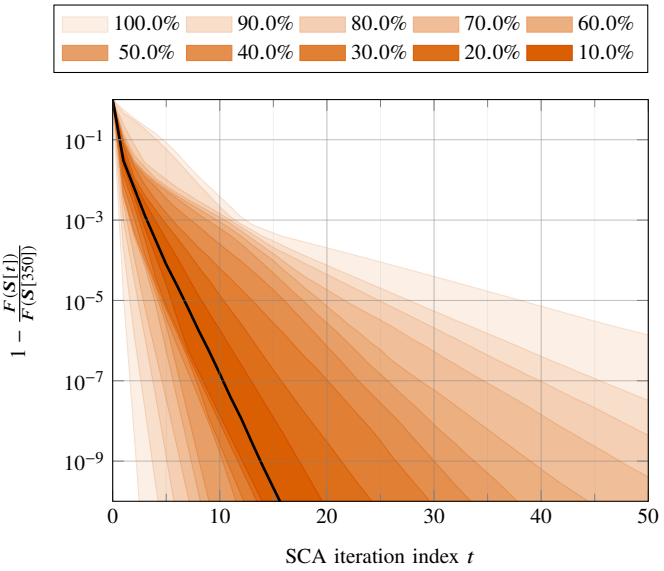

Fig. 6. Distribution of the distance to optimal rate after each iteration t, i.e. the relative difference between the data rate after iteration t and the data rate after iteration 350. The black line shows the median distance to optimal rate, and the shaded areas show different percentiles of the distance to optimal rate distribution centered around the median.

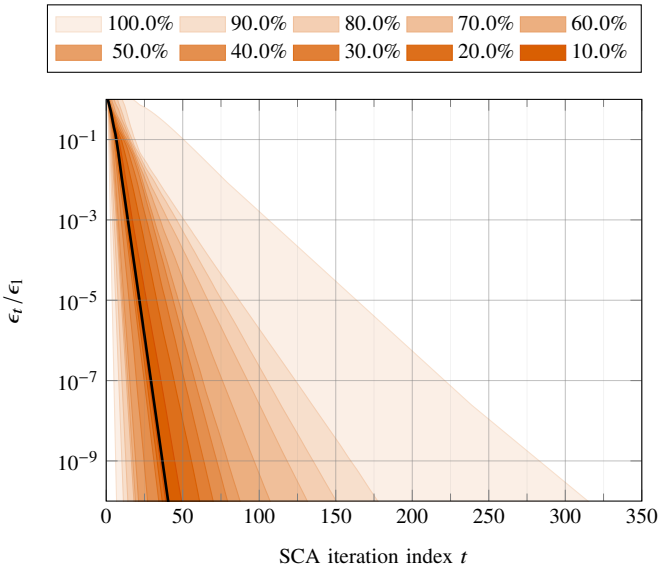

Fig. 7. Distribution of the relative KKT error ϵ_t after each iteration t. The black line shows the median relative KKT error, and the shaded areas show different percentiles of the relative KKT error distribution centered around the median.

fact that the obtained solution after 350 iterations yields a very small KKT error — more than 10 orders of magnitude smaller than the KKT error obtained after the first iteration — implies that it lies close to a stationary point of problem (56) [40, Theorem 3.2]. It can thus be concluded that, for the considered systems, only 10 to 20 iterations of the SCA algorithm are needed to obtain an accurate solution to problem (56).

VI. Conclusion & Future Work

In this paper, a new algorithm to simultaneously optimize receiver-side channel shortening PTEQ filter coefficients and transmit power allocation in OFDM and DMT systems with ZP or CP has been presented. The algorithm provably converges to a stationary point of the considered rate maximization problem, and requires only few iterations to achieve sufficient accuracy. Moreover, using this resource allocation method, it has been demonstrated that iterative water filling schemes can achieve good performance when the ISI/ICI is sufficiently suppressed by the PTEQ filter. In addition, transmitter-side channel shortening PTPC has been considered. A duality result linking OFDM/DMT systems with PTPC to OFDM/DMT systems with PTEQ has been provided. With this duality result in hand, PTPC systems can take full advantage of the straightforward FIR filter optimization in PTEQ systems, as well as of the developed resource allocation algorithm. Simulation results have shown that the performance obtained for OFDM/DMT systems with PTEQ is nearly indistinguishable from that obtained for OFDM/DMT systems with PTPC, making PTPC an interesting alternative channel shortening strategy in scenarios where implementing PTEQ is either difficult or costly.

In future work, the presented algorithms and results will be extended to multi-user systems. The joint PTEQ filter optimization and resource allocation algorithm from Section III readily extends to multi-user uplink systems — where PTEQ is thus applied at the base station — as the surrogate problem from Section III-B will be separable into subproblems that can be solved using the algorithm from Section III-C. Moreover, the results from Section IV-B can likely be generalized to establish a PTEQ-PTPC duality between multi-user uplink systems with PTEQ and multi-user downlink systems with PTPC, provided that a single base station-wide aggregate transmit power constraint is considered. If multi-user downlink systems with PTPC and per antenna or per line power constraints are considered — as would be customary in DSL networks [20], [35], [41] — PTEQ-PTPC duality can likely still be used to show an equivalence between the Lagrangian of the resulting rate maximization problem and the Lagrangian of a rate maximization problem in a multi-user uplink system with PTEQ, similar to e.g. [35], [41]. However, algorithms that are based on evaluating the Lagrange dual function by maximizing the Lagrangian of a rate maximization problem in a multi-user uplink system with PTEQ will likely exhibit a prohibitively high computational complexity, as they will require evaluating the SINR γ_n of each subcarrier n in each iteration of their inner loop. Overcoming this complexity obstacle will then represent an additional challenge.

Appendix
Proof of Proposition 2

Proof:

a) $\mathcal{S}$ is non-empty, closed, convex: Trivially satisfied, as

$$\mathcal{S} = \left\{ \boldsymbol{S} \in \mathbb{R}_+^N \mid \sum\nolimits_{n=0}^{N-1} S_n \, |\mathrm{col}_n \, \mathbf{T}|^2 \leq s P_{\text{sample}} \right\}.$$

b) $F \in C^1$ on an open set $\mathcal{V} \supset \mathcal{S}$: As the function $\log_2(1+\Gamma^{-1}\bullet)$ is differentiable on $\mathbb{R}_{++} - \{\Gamma\}$, the result can be proven by constructing an open set $\mathcal{V} \supset \mathcal{S}$ on which $\gamma_n \in C^1$ and $\gamma_n > -\Gamma$ for each $n \in \{0, \ldots, N-1\}$. By restricting $\mathcal{V}$ to be of the form

$$\mathcal{V} = \left\{ \boldsymbol{V} \in \mathbb{R}_{++}^N - \{[\epsilon, \ldots, \epsilon]^{\mathrm{T}}\} \mid \sum\nolimits_{n=0}^{N-1} V_n \, |\mathrm{col}_n \, \mathbf{T}|^2 < 2 s P_{\text{sample}} \right\},$$

the proof simplifies to finding an $\epsilon > 0$ such that on $\mathcal{V}$, both $\gamma_n \in C^1$ and $\gamma_n > -\Gamma$ for each $n \in \{0, \ldots, N-1\}$. It will be proven that if ϵ is chosen such that

$$\epsilon < \min_n \frac{\lambda_{\min}\big(\sigma^2 \, \underline{\mathbf{R}}_n \, \underline{\mathbf{R}}_n^{\mathcal{H}}\big)}{\Gamma^{-1} \, |\boldsymbol{h}_n|^2 + \lambda_{\max}\big(\sum_{m=0}^{N-1} \mathbb{H}_{nm} \, \mathbb{H}_{nm}^{\mathcal{H}}\big)}, \tag{61}$$

where $\lambda_{\min}(\mathbf{A})$ and $\lambda_{\max}(\mathbf{A})$ denote the smallest and largest eigenvalue of $\mathbf{A}$ respectively, both conditions are satisfied.

As for the condition that $\gamma_n > -\Gamma$ on $\mathcal{V}$, from (61) it follows that for each $n \in \{0, \ldots, N-1\}$

$$\epsilon \Gamma^{-1} \, |\boldsymbol{h}_n|^2 < \lambda_{\min}\big(\sigma^2 \, \underline{\mathbf{R}}_n \, \underline{\mathbf{R}}_n^{\mathcal{H}}\big) + \lambda_{\min}\Big(- \sum_{m=0}^{N-1} \epsilon \, \mathbb{H}_{nm} \, \mathbb{H}_{nm}^{\mathcal{H}} \Big).$$

Weyl's inequality then implies that for each $n \in \{0, \ldots, N-1\}$

$$\epsilon \Gamma^{-1} \, |\boldsymbol{h}_n|^2 < \lambda_{\min}\big(\boldsymbol{\Psi}_n(-[\epsilon, \ldots, \epsilon]^{\mathrm{T}})\big) = \inf_{\boldsymbol{V} \in \mathcal{V}} \lambda_{\min}\big(\boldsymbol{\Psi}_n(\boldsymbol{V})\big), \tag{62}$$

which is equivalent to

$$\epsilon \, |\boldsymbol{h}_n|^2 \sup_{\boldsymbol{V} \in \mathcal{V}} \lambda_{\max}\big(\boldsymbol{\Psi}_n(\boldsymbol{V})^{-1}\big) < \Gamma. \tag{63}$$

As $\boldsymbol{b}^{\mathcal{H}} \mathbf{A} \, \boldsymbol{b} \leq \lambda_{\max}(\mathbf{A}) \, |\boldsymbol{b}|^2$ for any invertible matrix $\mathbf{A}$ and vector $\boldsymbol{b}$, equation (63) yields

$$-\Gamma < -\epsilon \sup_{\boldsymbol{V} \in \mathcal{V}} \left\{ \boldsymbol{h}_n^{\mathcal{H}} \, \boldsymbol{\Psi}_n(\boldsymbol{V})^{-1} \, \boldsymbol{h}_n \right\}, \tag{64}$$

implying that for each $n \in \{0, \ldots, N-1\}$

$$-\Gamma < \inf_{\boldsymbol{V} \in \mathcal{V}} \gamma_n(\boldsymbol{V}). \tag{65}$$

Returning to the condition that $\gamma_n \in C^1$ on $\mathcal{V}$, as $f, g \in C^1 \implies f \, g \in C^1$, it suffices to establish continuous differentiability for $\boldsymbol{h}_n^{\mathcal{H}} \, \boldsymbol{\Psi}_n^{-1} \, \boldsymbol{h}_n$. To do so, it is noted that the inverse of any invertible matrix $\mathbf{A}$ can be written as

$$\mathbf{A}^{-1} = \frac{1}{\det \mathbf{A}} \mathbf{C} \tag{66}$$

with $\mathbf{C}$ the cofactor matrix of $\mathbf{A}$, the elements of which are given by the (negative) determinant of specific sub-matrices of $\mathbf{A}$. Using the fact that the determinant of any matrix is a polynomial function of the matrix elements, it can then be seen that there exists a real polynomial function $P : \mathbb{R}^N \to \mathbb{R}$ such that

$$\boldsymbol{h}_n^{\mathcal{H}} \, \boldsymbol{\Psi}_n^{-1} \, \boldsymbol{h}_n = \frac{P}{\det \boldsymbol{\Psi}_n}. \tag{67}$$

As both P and $\det \boldsymbol{\Psi}_n$ are continuously differentiable functions, and as it is known from (62) that $0 < \det \boldsymbol{\Psi}_n$ on $\mathcal{V}$, it can be concluded that $\boldsymbol{h}_n^{\mathcal{H}} \, \boldsymbol{\Psi}_n^{-1} \, \boldsymbol{h}_n$ — and by extension γ_n — is continuously differentiable on $\mathcal{V}$.

c) ∇F is Lipschitz continuous on $\mathcal{S}$: Using the same arguments as in the proof of **P1.b**, it can be seen that each $(n+1)$-th partial derivative of F — which is given in (68) — is itself continuously differentiable on $\mathcal{V}$. As continuous differentiability implies Lipschitz continuity, it is concluded that ∇F is Lipschitz continuous on $\mathcal{S}$.

d) F is bounded from above on $\mathcal{S}$: Trivially satisfied, as

$$\max_{\boldsymbol{S}\in\mathcal{S}} \gamma_n(\boldsymbol{S}) \leq \frac{sP_{\text{sample}}}{|\text{col}_n\,\mathbf{T}|^2}\, \boldsymbol{h}_n^{\mathcal{H}} (\sigma^2\, \underline{\mathbf{R}}_n\, \underline{\mathbf{R}}_n^{\mathcal{H}})^{-1}\, \boldsymbol{h}_n, \quad \forall n. \tag{69}$$

e) $\tilde{F}(\bullet|\tilde{\boldsymbol{S}}) \in C^1$ on an open set $\mathcal{V} \supset \mathcal{S}$, $\forall \tilde{\boldsymbol{S}} \in \mathcal{S}$: As $\sigma^2\, \underline{\mathbf{R}}_n\, \underline{\mathbf{R}}_n^{\mathcal{H}} \succ 0$, it is evident from their definitions in (38) that both ψ_n and a_n are positive and bounded on $\mathcal{S}$. Letting $\psi_n^{\max} \in \mathbb{R}_+$ denote a finite upper bound for ψ_n on $\mathcal{S}$, it can be seen that $\tilde{F}(\bullet|\tilde{\boldsymbol{S}}) \in C^1$ on the open set

$$\mathbb{R}_{++}^N - \left\{\Gamma\left[(\psi_0^{\max})^{-1}, \ldots, (\psi_{N-1}^{\max})^{-1}\right]^{\mathrm{T}}\right\}. \tag{70}$$

f) $\tilde{F}(\bullet|\tilde{\boldsymbol{S}})$ is uniformly strongly concave, $\forall \tilde{\boldsymbol{S}} \in \mathcal{S}$: The $(n+1)$-th partial derivative of $\tilde{F}(\bullet|\tilde{\boldsymbol{S}})$ is given as

$$\frac{\partial}{\partial S_n} \tilde{F}(\bullet|\tilde{\boldsymbol{S}}) = \frac{\psi_n(\tilde{\boldsymbol{S}})/\log(2)}{\Gamma + S_n\, \psi_n(\tilde{\boldsymbol{S}})} - a_n(\tilde{\boldsymbol{S}}). \tag{71}$$

Using the same arguments as in the proof of **P1.e**, it is proven that $\tilde{F}(\bullet|\tilde{\boldsymbol{S}}) \in C^2$ on an open set $\mathcal{V} \supset \mathcal{S}$. The Hessian of $\tilde{F}(\bullet|\tilde{\boldsymbol{S}})$ is a diagonal matrix that is defined by

$$\frac{\partial^2}{\partial S_n^2} \tilde{F}(\bullet|\tilde{\boldsymbol{S}}) = -\frac{\psi_n(\tilde{\boldsymbol{S}})^2/\log(2)}{\left(\Gamma + S_n\, \psi_n(\tilde{\boldsymbol{S}})\right)^2}. \tag{72}$$

Strong concavity of $\tilde{F}(\bullet|\tilde{\boldsymbol{S}})$ can thus be proven by establishing an upper bound on the Hessian's diagonal elements, which in turn requires establishing a positive upper bound and a strictly positive lower bound for ψ_n on $\mathcal{S}$. An upper bound for ψ_n on $\mathcal{S}$ was already established as part of the proof for **P1.e**. The fact that a strictly positive lower bound for ψ_n exists on $\mathcal{S}$ is due to the eigenvalues of $\boldsymbol{\Psi}_i$ being bounded on $\mathcal{S}$.

g) $\nabla F(\tilde{\boldsymbol{S}}) = \nabla \tilde{F}(\bullet|\tilde{\boldsymbol{S}})\big|_{\boldsymbol{S}=\tilde{\boldsymbol{S}}}$, $\forall \tilde{\boldsymbol{S}} \in \mathcal{S}$: Substituting $a_n(\tilde{\boldsymbol{S}})$ in (71) with its definition in (38b) and setting $\boldsymbol{S} = \tilde{\boldsymbol{S}}$ yields (68).

h) $\nabla \tilde{F}(\boldsymbol{S}|\bullet)$ is Lipschitz continuous on $\mathcal{S}$ for all $\boldsymbol{S} \in \mathcal{S}$: Using the same arguments as in the proof of **P1.b**, it can be proven that each $(n+1)$-th partial derivative of $\tilde{F}(\boldsymbol{S}|\bullet)$ — which is given in (73a)-(73d) — is itself continuously differentiable on $\mathcal{V}$. As continuous differentiability implies Lipschitz continuity, it is concluded that $\nabla \tilde{F}(\boldsymbol{S}|\bullet)$ is Lipschitz continuous on $\mathcal{S}$.

■

Acknowledgment

The authors would like to thank Wouter Lanneer for proof reading the manuscript and for his constructive criticism.

References

[1] ITU-T Study Group 15, "Fast access to subscriber terminals (G.fast) – Power spectral density specification," International Telecommunication Union, Tech. Rep., 2014.

[2] ——, "Fast access to subscriber terminals (G.fast) – Physical layer specification," International Telecommunication Union, Tech. Rep. ITU-T G.9701, 2015.

[3] R. Strobel and W. Utschick, "Coexistence of G.fast and VDSL in FTTDP and FTTC deployments," in *Proc. 23rd European Signal Processing Conference (EUSIPCO)*, Aug. 2015, pp. 1103–1107.

[4] F. Effenberger, "Future broadband access networks," *Proceedings of the IEEE*, vol. 104, no. 11, pp. 2078–2081, Nov. 2016.

[5] R. Strobel and V. Oksman, "Line grouping for crosstalk avoidance," US Patent US20 180 041 246A1, Feb., 2018.

[6] D. Hincapie, M. Leibiger, and E. Oswald, "Roll-out of giga-bit copper: Impact-analysis of deploying G.fast in FTTC access networks," in *Proc. 12th ITG-Symposium; Broadband Coverage in Germany*, Apr. 2018, pp. 1–6.

[7] F. Mazzenga and R. Giuliano, "Analysis of zero-forcing vectoring for VDSL2 and long reach VDSL technologies," *IEEE Transactions on Communications*, vol. 67, no. 11, pp. 7811–7823, Nov. 2019.

[8] J. Chow, J. Tu, and J. Cioffi, "A discrete multitone transceiver system for HDSL applications," *IEEE Journal on Selected Areas in Communications*, vol. 9, no. 6, pp. 895–908, Aug. 1991.

[9] K. V. Acker, G. Leus, M. Moonen, O. v. d. Wiel, and T. Pollet, "Per tone equalization for DMT-based systems," *IEEE Transactions on Communications*, vol. 49, no. 1, pp. 109–119, Jan. 2001.

[10] M. Wolkerstorfer, P. Tsiaflakis, M. Moonen, and D. Statovci, "Joint power-loading and cyclic prefix length optimization for OFDM-based power line communication," in *Proc. IEEE International Conference on Acoustics, Speech and Signal Processing*, May 2013, pp. 4688–4692.

[11] W. Henkel, G. Taubock, P. Odling, P. Borjesson, and N. Petersson, "The cyclic prefix of OFDM/DMT - An analysis," in *Proc. International Zurich Seminar on Broadband Communications Access - Transmission - Networking (Cat. No.02TH8599)*, Feb. 2002, pp. 22–22.

[12] M. Wolkerstorfer, M. Moonen, and D. Statovci, "Multiuser spectrum balancing under inter-carrier interference," *IEEE Communications Letters*, vol. 16, no. 10, pp. 1560–1563, Oct. 2012.

[13] V. M. K. Chan and W. Yu, "Multiuser spectrum optimization for discrete multitone systems with asynchronous crosstalk," *IEEE Transactions on Signal Processing*, vol. 55, no. 11, pp. 5425–5435, Nov. 2007.

[14] R. Cendrillon, J. Huang, M. Chiang, and M. Moonen, "Autonomous spectrum balancing for digital subscriber lines," *IEEE Transactions on Signal Processing*, vol. 55, no. 8, pp. 4241–4257, Aug. 2007.

[15] W. Yu, "Multiuser water-filling in the presence of crosstalk," in *Proc. Information Theory and Applications Workshop*, La Jolla, CA, USA, Jan. 2007, pp. 414–420.

[16] P. K. Pandey, M. Moonen, and L. Deneire, "Sparse approximation based resource allocation in DSL/DMT transceivers with per-tone equalization," *Signal Processing*, vol. 95, pp. 43–48, Feb. 2014.

[17] I. Singh and K. Giridhar, "Enhancement in spectral efficiency using transmit-side channel shortener for MISO-OFDM systems," *IEEE Signal Processing Letters*, vol. 21, no. 6, pp. 712–716, Jun. 2014.

[18] C.-Y. Chen and S.-M. Phoong, "Per tone shaping filters for DMT transmitters," in *Proc. IEEE International Conference on Acoustics, Speech, and Signal Processing*, vol. 4, Montreal, Que., Canada, 2004, pp. 1061–1064.

[19] W. Yu and T. Lan, "Transmitter optimization for the multi-antenna downlink with per-antenna power constraints," *IEEE Transactions on Signal Processing*, vol. 55, no. 6, pp. 2646–2660, Jun. 2007.

[20] V. Le Nir, M. Moonen, J. Verlinden, and M. Guenach, "Optimal power allocation for downstream xDSL with per-modem total power constraints: broadcast channel optimal spectrum balancing (BC-OSB)," *IEEE Transactions on Signal Processing*, vol. 57, no. 2, pp. 690–697, Feb. 2009.

[21] R. Hunger, M. Joham, and W. Utschick, "On the MSE-Duality of the broadcast channel and the multiple access channel," *IEEE Transactions on Signal Processing*, vol. 57, no. 2, pp. 698–713, Feb. 2009.

[22] B. Muquet, Zhengdao Wang, G. B. Giannakis, M. d. Courville, and P. Duhamel, "Cyclic prefixing or zero padding for wireless multicarrier transmissions?" *IEEE Transactions on Communications*, vol. 50, no. 12, pp. 2136–2148, Dec. 2002.

[23] N. U. Ahmed and K. R. Rao, *Orthogonal transforms for digital signal processing*. Berlin, Heidelberg: Springer-Verlag, 1975.

$$\frac{\partial F}{\partial S_n} = -\sum_{m=0}^{N-1} \frac{S_m/\log(2)}{\Gamma + \gamma_m(\boldsymbol{S})} \left|\mathbb{H}_{mn}^{\mathcal{H}}\, \boldsymbol{\Psi}_m(\boldsymbol{S})^{-1}\, \boldsymbol{h}_m\right|^2 + \frac{1/\log(2)}{\Gamma + \gamma_n(\boldsymbol{S})}\, \boldsymbol{h}_n^{\mathcal{H}}\, \boldsymbol{\Psi}_n(\boldsymbol{S})^{-1}\, \boldsymbol{h}_n \tag{68}$$

$$\frac{\partial}{\partial \tilde{S}_n} \tilde{F}(\boldsymbol{S}|\bullet) = -\sum_{m=0}^{N-1} \left(\frac{S_m \left|\mathbb{H}_{mn}^{\mathcal{H}}\, \boldsymbol{\Psi}_m(\tilde{\boldsymbol{S}})^{-1}\, \boldsymbol{h}_m\right|^2}{\Gamma + S_m\, \psi_m(\tilde{\boldsymbol{S}})} + S_m \frac{\partial a_m}{\partial \tilde{S}_n} \right) \tag{73a}$$

$$\frac{\partial a_m}{\partial \tilde{S}_n} = \sum_{o=0}^{N-1} \left[\left|\mathbb{H}_{om}^{\mathcal{H}}\, \boldsymbol{\Psi}_o(\tilde{\boldsymbol{S}})^{-1}\, \boldsymbol{h}_o\right|^2 \frac{\partial}{\partial \tilde{S}_n} \frac{\tilde{S}_o/\log(2)}{\Gamma + \gamma_o(\tilde{\boldsymbol{S}})} + \frac{\tilde{S}_o/\log(2)}{\Gamma + \gamma_o(\tilde{\boldsymbol{S}})} \frac{\partial}{\partial \tilde{S}_n} \left|\mathbb{H}_{om}^{\mathcal{H}}\, \boldsymbol{\Psi}_o(\tilde{\boldsymbol{S}})^{-1}\, \boldsymbol{h}_o\right|^2 \right] \tag{73b}$$

$$\frac{\partial}{\partial \tilde{S}_n} \frac{\tilde{S}_o/\log(2)}{\Gamma + \gamma_o(\tilde{\boldsymbol{S}})} = -\left(\Gamma + \gamma_o(\tilde{\boldsymbol{S}})\right)^{-2}/\log(2) \begin{cases} \tilde{S}_o \left|\mathbb{H}_{on}^{\mathcal{H}}\, \boldsymbol{\Psi}_o(\tilde{\boldsymbol{S}})^{-1}\, \boldsymbol{h}_o\right|^2 - \Gamma - \gamma_o(\tilde{\boldsymbol{S}}) & \text{when } n = o \\ \tilde{S}_o \left|\mathbb{H}_{on}^{\mathcal{H}}\, \boldsymbol{\Psi}_o(\tilde{\boldsymbol{S}})^{-1}\, \boldsymbol{h}_o\right|^2 & \text{when } n \neq o \end{cases} \tag{73c}$$

$$\frac{\partial}{\partial \tilde{S}_n} \left|\mathbb{H}_{om}^{\mathcal{H}}\, \boldsymbol{\Psi}_o(\tilde{\boldsymbol{S}})^{-1}\, \boldsymbol{h}_o\right|^2 = 2\,\Re\left\{ \boldsymbol{h}_o^{\mathcal{H}}\, \boldsymbol{\Psi}_o(\tilde{\boldsymbol{S}})^{-1}\, \mathbb{H}_{on}\, \mathbb{H}_{on}^{\mathcal{H}}\, \boldsymbol{\Psi}_o(\tilde{\boldsymbol{S}})^{-1}\, \mathbb{H}_{om}\, \mathbb{H}_{om}^{\mathcal{H}}\, \boldsymbol{\Psi}_o(\tilde{\boldsymbol{S}})^{-1}\, \boldsymbol{h}_o \right\} \tag{73d}$$

[24] W. A. Martins, F. Cruz–Roldán, M. Moonen, and P. S. Ramirez Diniz, "Intersymbol and intercarrier interference in OFDM transmissions through highly dispersive channels," in *Proc. 27th European Signal Processing Conference (EUSIPCO)*, Sep. 2019, pp. 1–5.

[25] ITU-T Study Group 15, "Very high speed digital subscriber line transceivers (VDSL)," International Telecommunication Union, Tech. Rep. ITU-T G.993.1, 2004.

[26] Y. Lin, C. Li, and S. Phoong, "A filterbank approach to window designs for multicarrier systems," *IEEE Circuits and Systems Magazine*, vol. 7, no. 1, pp. 19–30, 2007.

[27] G. Forney and M. Eyuboglu, "Combined equalization and coding using precoding," *IEEE Communications Magazine*, vol. 29, no. 12, pp. 25–34, Dec. 1991.

[28] P. Chow, J. Cioffi, and J. Bingham, "A practical discrete multitone transceiver loading algorithm for data transmission over spectrally shaped channels," *IEEE Transactions on Communications*, vol. 43, no. 2/3/4, pp. 773–775, Feb. 1995.

[29] A. Suls, J. Verdyck, M. Moonen, and M. Moeneclaey, "Modified SNR gap approximation for resource allocation in LDPC-coded multicarrier systems," *IEEE Access*, vol. 8, pp. 1577–1586, 2020.

[30] Z.-Q. Luo and S. Zhang, "Dynamic spectrum management: complexity and duality," *IEEE Journal of Selected Topics in Signal Processing*, vol. 2, no. 1, pp. 57–73, Feb. 2008.

[31] F. Facchinei, G. Scutari, and S. Sagratella, "Parallel selective algorithms for nonconvex big data optimization," *IEEE Transactions on Signal Processing*, vol. 63, no. 7, pp. 1874–1889, Apr. 2015.

[32] Y. Yang and M. Pesavento, "A unified successive pseudoconvex approximation framework," *IEEE Transactions on Signal Processing*, vol. 65, no. 13, pp. 3313–3328, Jul. 2017.

[33] G. Scutari, F. Facchinei, P. Song, D. P. Palomar, and J. Pang, "Decomposition by partial linearization: parallel optimization of multi-agent systems," *IEEE Transactions on Signal Processing*, vol. 62, no. 3, pp. 641–656, Feb. 2014.

[34] L. Cannelli, F. Facchinei, V. Kungurtsev, and G. Scutari, "Asynchronous Parallel Algorithms for Nonconvex Big-Data Optimization. Part II: Complexity and Numerical Results," *arXiv:1701.04900 [math]*, Jan. 2017, arXiv: 1701.04900.

[35] J. Verdyck, W. Lanneer, P. Tsiaflakis, W. Coomans, P. Patrinos, and M. Moonen, "Optimal dynamic spectrum management algorithms for multi-user full-duplex DSL," *IEEE Access*, vol. 7, pp. 106 600–106 616, 2019.

[36] W. Yu, W. Rhee, S. Boyd, and J. M. Cioffi, "Iterative water-filling for Gaussian vector multiple-access channels," *IEEE Transactions on Information Theory*, vol. 50, no. 1, pp. 145–152, Jan. 2004.

[37] S. Huberman, C. Leung, and T. Le-Ngoc, "Constant offset autonomous spectrum balancing using multiple reference lines for VDSL," *IEEE Transactions on Signal Processing*, vol. 60, no. 12, pp. 6719–6723, Dec. 2012.

[38] D. Acatauassu, S. Höst, C. Lu, M. Berg, A. Klautau, and P. O. Börjesson, "Simple and causal twisted-pair channel models for G.fast systems," in *Proc. IEEE Global Communications Conference (GLOBECOM)*, Dec. 2013, pp. 2834–2839.

[39] N. Al-Dhahir and J. Cioffi, "Efficiently computed reduced-parameter input-aided MMSE equalizers for ML detection: a unified approach," *IEEE Transactions on Information Theory*, vol. 42, no. 3, pp. 903–915, May 1996.

[40] J. Dutta, K. Deb, R. Tulshyan, and R. Arora, "Approximate KKT points and a proximity measure for termination," *Journal of Global Optimization*, vol. 56, no. 4, pp. 1463–1499, Aug. 2013.

[41] W. Lanneer, P. Tsiaflakis, J. Maes, and M. Moonen, "Linear and nonlinear precoding based dynamic spectrum management for downstream vectored G.fast transmission," *IEEE Transactions on Communications*, vol. 65, no. 3, pp. 1247–1259, Mar. 2017.